Geochemistry, Geophysics, Geosystems

RESEARCH ARTICLE
10.1029/2020GC009091

Key Points:
- Southward tearing of oceanic lithosphere from continental lithosphere of the Indian plate occurred in central Myanmar
- Active slab detachment triggers both arc-like and OIB-like Quaternary basaltic volcanism during highly oblique continental subduction
- An exotic asthenosphere layer beneath the Burmese microplate flowed from central and SE Tibet

Supporting Information:
- Supporting Information S1
- Table S1

Correspondence to:
L. Y. Zhang,
zly@itpcas.ac.cn

Citation:
Zhang, L. Y., Fan, W. M., Ding, L., Ducea, M. N., Pullen, A., Li, J. X., et al. (2020). Quaternary volcanism in Myanmar: A record of Indian slab tearing in a transition zone from oceanic to continental subduction. *Geochemistry, Geophysics, Geosystems*, *21*, e2020GC009091. https://doi.org/10.1029/2020GC009091

Received 8 APR 2020
Accepted 20 JUN 2020
Accepted article online 23 JUN 2020

Quaternary Volcanism in Myanmar: A Record of Indian Slab Tearing in a Transition Zone From Oceanic to Continental Subduction

L. Y. Zhang[1,2], W. M. Fan[1,2,3], L. Ding[1,2], M. N. Ducea[4,5], A. Pullen[6], J. X. Li[1,2], Y. L. Sun[1,2], Y. H. Yue[1], F. L. Cai[1,2], C. Wang[1], T. P. Peng[2,7], and Kyaing Sein[8]

[1]Key Laboratory of Continental Collision and Plateau Uplift, Institute of Tibetan Plateau Research, Chinese Academy of Sciences, Beijing, China, [2]Center for Excellence in Tibetan Plateau Earth Sciences, Chinese Academy of Sciences, Beijing, China, [3]College of Earth and Planetary Sciences, University of Chinese Academy of Sciences, Beijing, China, [4]Department of Geosciences, University of Arizona, Tucson, AZ, USA, [5]Facultatea de Geologie si Geofizica, Universitatea Bucuresti, Bucuresti, Romania, [6]Department of Environmental Engineering and Earth Sciences, Clemson University, Clemson, SC, USA, [7]State Key Laboratory of Isotope Geochemistry, Guangzhou Institute of Geochemistry, Chinese Academy of Sciences, Guangzhou, China, [8]Myanmar Geosciences Society, Yangon, Myanmar

Abstract Magmatic processes that occur during the transition from oceanic to continental subduction and collision in orogens are critical and still poorly resolved. Oceanic slab detachment in particular is hypothesized to mark a fundamental change in magmatism and deformation within an orogen. Here, we report on two Quaternary volcanic centers of Myanmar that may help us better understand the process of slab detachment. The Monywa volcanic rocks are composed of low-K tholeiitic, medium-K calk-alkaline, and high-K to shoshonitic basalts with arc signatures, while the Singu volcanic rocks show geochemical characteristics similar to asthenosphere-derived magmas. These volcanic rocks have low Os concentrations but extremely high $^{187}Os/^{186}Os_i$ ratios (0.1498 to 0.3824) due to minor (<4%) crustal contamination. The Monywa arc-like rocks were generated by small degrees of partial melting of subduction-modified asthenospheric mantle at variable depths from the spinel to garnet stability fields. Distinct from the Monywa arc-like rocks ($^{87}Sr/^{86}Sr_i$ = 0.7043 to 0.7047; εNd_i = +2.3 to +4.7), the Singu OIB-like rocks exhibit higher $^{87}Sr/^{86}Sr_i$ (0.7056 to 0.7064) and lower εNd_i (+0.8 to +1.6) values. These isotopic characteristics indicate a large contribution of an isotopically enriched asthenosphere layer beneath the Burmese microplate, which possibly flowed from SE Tibet. We interpret that this short-lived, small-scale, and low-degree melting Quaternary volcanism in Myanmar was triggered by its position above a slab window resulting from the tearing of the oceanic lithosphere from buoyant continental lithosphere of the Indian plate.

1. Introduction

An important tectonic magmatic change during a Wilson cycle is expected to occur at the transition from oceanic to continental subduction and continental collision. Various segments of Tethyan orogen formed as the result of the Tethyan Ocean consumption from western Europe into Asia are great examples of areas that underwent such a transition at one time or another during the Cenozoic or Mesozoic. Not all segments were magmatically active through this transition, but those who were provide the geologic record of major changes in the convergence process. Unlike the oceanic crust, which is easily subducted along most convergent margins, the continental crust is generally more buoyant and thus resists subduction. However, ultrahigh pressure metamorphic terrains demonstrate that continental crust can, at minimum, partially subduct to depths of 150–200 km (e.g., Ducea, 2016), and seismic observations strongly suggest that they can be buried to >300 km (Kind & Yuan, 2010; Sippl et al., 2013; Zhao et al., 2010). The buoyancy forces during continental subduction and strength limits of the lithosphere favor a scenario in which the oceanic lithosphere detaches from the neighboring continental lithosphere (von Blanckenburg & Davies, 1995). Slab detachment results in asthenosphere upwelling through the newly developed slab window and a perturbation to the thermal structure of the preexisting mantle wedge. This results in a source change from melting the predominately metasomatized mantle wedge of the overriding plate to melting the asthenosphere itself (Davies & von Blanckenburg, 1995). This change in magmatism is widely used to delineate the timing and spatial distribution of slab detachment in the Mediterranean region (e.g., Dilek &

Altunkaynak, 2009; Prelević et al., 2015). The slab detachment model also has been applied to explain the early Cenozoic tectonic and magmatic evolution in the India-Asia collision zone (e.g., Chung et al., 2005; Ji et al., 2016; Lee et al., 2009; Mahéo et al., 2002; Zhu et al., 2015). When invoking "slab detachment" as a trigger, however, caution must be exercised without convincing geophysical and geological observations (Garzanti et al., 2018; Niu, 2017).

By looking at an example from an active slab detachment, it is possible to critically evaluate ancient ones; unfortunately, very few modern or very young such transitions exist. The Burmese microplate is an exception located above a transition from oceanic to continental lithosphere of the subducting Indian plate (Figure 1). Continental lithosphere of the Indian plate is being (partially) subducted beneath the Himalayan-Tibetan orogen of the Eurasian plate (e.g., Kind & Yuan, 2010; Shi et al., 2015; Xu et al., 2017; Zhao et al., 2010), whereas oceanic lithosphere outboard of the Indian plate is subducting along the Andaman-Sunda-Java trench to the east (e.g., Pesicek et al., 2010; Replumaz et al., 2010; Syacuse & Abers, 2007). Because of this favorable along plate transition, slab detachment is postulated and, at some point, expected beneath the Burmese microplate (Figure 1).

Understanding the different mantle melting processes (i.e., fluid fluxing and decompression) and determining their relative importance in the generation of primary basalts is important for geodynamic research. Quaternary volcanic rocks in central Myanmar are compositionally different from similar age volcanic rocks along the Andaman-Sunda-Java arc to the S-SE (Figure 1) and have noticeably low production rates and lack a well-defined volcanic belt (Figure 2a; Lee et al., 2016; Maury et al., 2004). For one reason, they are basaltic, thus representing ideal candidates to study mantle melting processes. In order to better understand mantle melting processes during oceanic to continental subduction transition, we investigated the chemical evolution of Quaternary volcanic rocks in the Burmese microplate. This paper presents whole-rock geochemical and Sr-Nd-Os isotopic data of the Monywa and Singu volcanics from central Myanmar to better understand this magma petrogenesis and geodynamic processes beneath the Burmese microplate. Our new results support a hypothesis of active slab tearing in the inferred transitional zone between oceanic and continental subduction on the Indian plate.

2. Geological Framework and Sample Descriptions

The Burmese microplate in Myanmar (Figure 2a) is bounded by the Churachandpur-Mao (CM) Fault to the west (e.g., Gahalaut et al., 2013) and Sagaing Fault to the east (Bertrand et al., 1998; Maurin et al., 2010). The Burmese microplate is juxtaposed to the India and Sunda plates (Figure 9a) and was formed along the Indo-Burmese Ranges (IBR) in the west (Licht et al., 2018; Maurin & Rangin, 2009) and the Mogok Metamorphic Belt (MMB) in the east (Mitchell et al., 2012; Searle et al., 2007).

The IBR is an accretionary complex that resulted from the subduction of Indian oceanic lithosphere under the Burmese active margin (e.g., Zhang et al., 2018). The IBR consists of an outer wedge composed of shortened Neogene Himalayan-sourced clastic sequences and an inner wedge primarily composed of Early Cretaceous ophiolites and Triassic schists covered by Upper Cretaceous-Eocene marine turbidites (Figure 9a; Licht et al., 2018; Zhang et al., 2018). The core of the inner wedge has a N-S strike-slip fault system with positive flower structures (Maurin & Rangin, 2009). Today, the inner wedge fault system is traversed by the CM dextral strike-slip fault system and accommodates a significant component (i.e., 50%) of the relative plate motion between the Indian and Sunda plates according to the recent GPS measurements of crustal deformation (Gahalaut et al., 2013).

The MMB extends for over 1,500 km along the western margin of the Shan Plateau, contains the Jurassic to Early Cretaceous subduction-related magmatism, a Tertiary magmatic and metamorphic event, and is generally considered to delineate the western margin of the rigid Sunda plate (Mitchell et al., 2012; Searle et al., 2007). The 1,200 km long Sagaing Fault extends across Myanmar from Yangon to the eastern Himalayan syntaxis (Figure 2a; Maurin et al., 2010) and in the south connects to the Andaman rift (Raju et al., 2004). The timing for onset of strike-slip deformation along the Sagaing Fault is unclear, but metamorphic ages of MMB gneisses indicate that the high-grade metamorphism and deformation had started by at least the middle Eocene (Licht et al., 2018; Searle et al., 2007). The total dextral displacement along the Sagaing Fault could exceed 400 km (e.g., Mitchell, 1993; Morley & Arboit, 2019). The current slip rate is nearly half that of the relative motion between India and Sunda plates (Maurin et al., 2010).

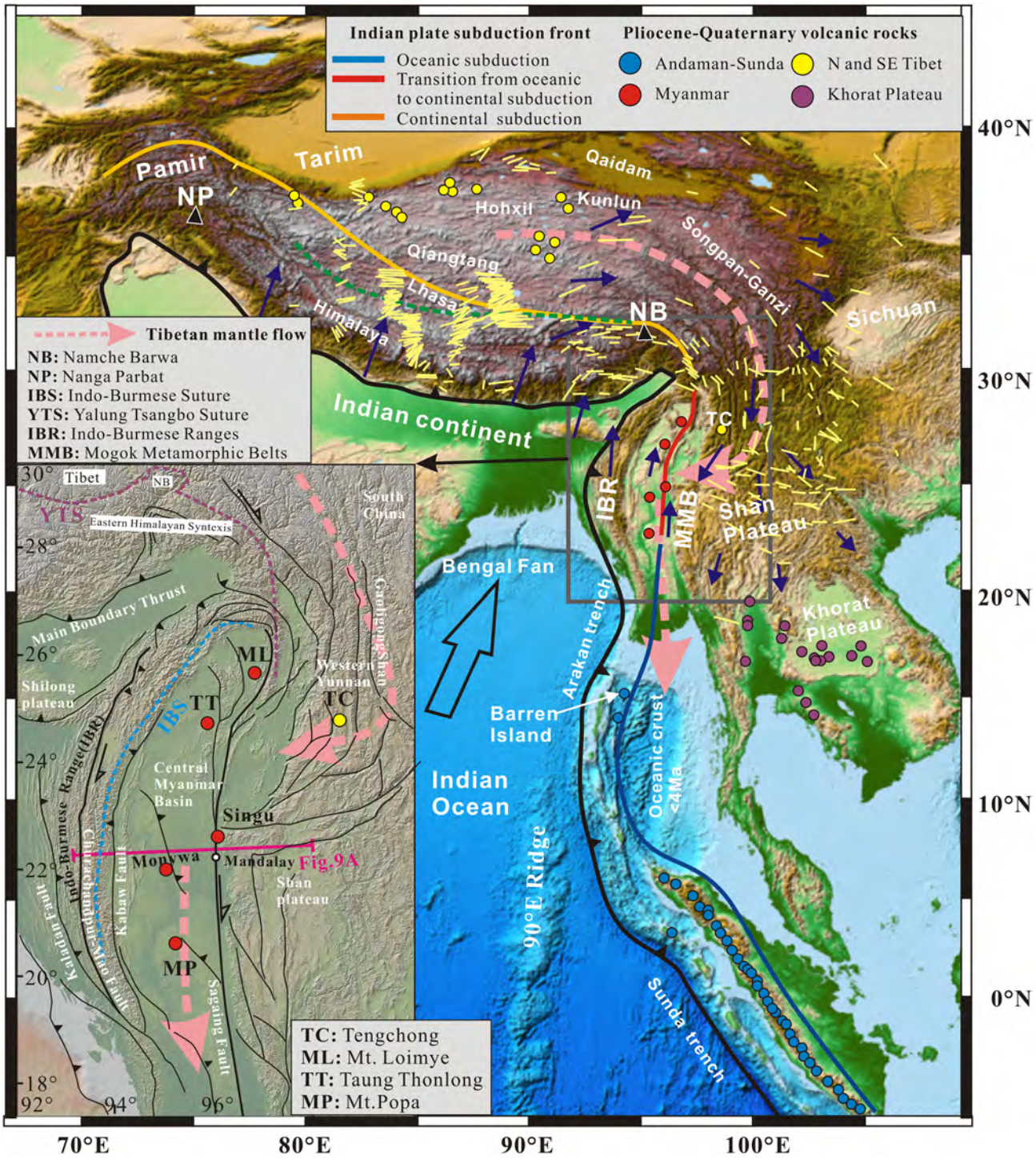

Figure 1. Digital Elevation Model (DEM) map of the NE Indian plate and the Eurasian plate (www.geomapapp.org). The blue solid line delineates the lowest edge of the subducted Indian ocean lithosphere beneath the Sunda-Andaman arcs (Pesicek et al., 2010; Replumaz et al., 2010; Syacuse & Abers, 2007), whereas the orange solid line delineates the Indian continental lithosphere subduction front beneath northern Tibet (e.g., Li et al., 2008) at depths of 100–200 km. The Indian lower crust subduction front is denoted by the green dashed line (Shi et al., 2015; Xu et al., 2017; Zhao et al., 2010). Orientations of Tibetan mantle flow (pink arrow) are marked by yellow lines from seismic anisotropy measurements (Kind & Yuan, 2010; Wang et al., 2008, and references therein). Surface displacements obtained from GPS observations are marked by dark blue arrows (Gahalaut et al., 2013; Maurin et al., 2010; Zhang et al., 2004). Distributions of the Pliocene-Quaternary volcanic centers are marked by filled circles in central and northern Tibet (Guo et al., 2006; Wang et al., 2016; Yang, 2011), Tengchong in SE Tibet (Tian et al., 2018; Zhou et al., 2011), Myanmar (Lee et al., 2016; Maury et al., 2004), Andaman-Sunda arcs (e.g., Chandrasekharam et al., 2009; Luhr & Haldar, 2006), and Khorat Plateau, Thailand (e.g., An et al., 2017).

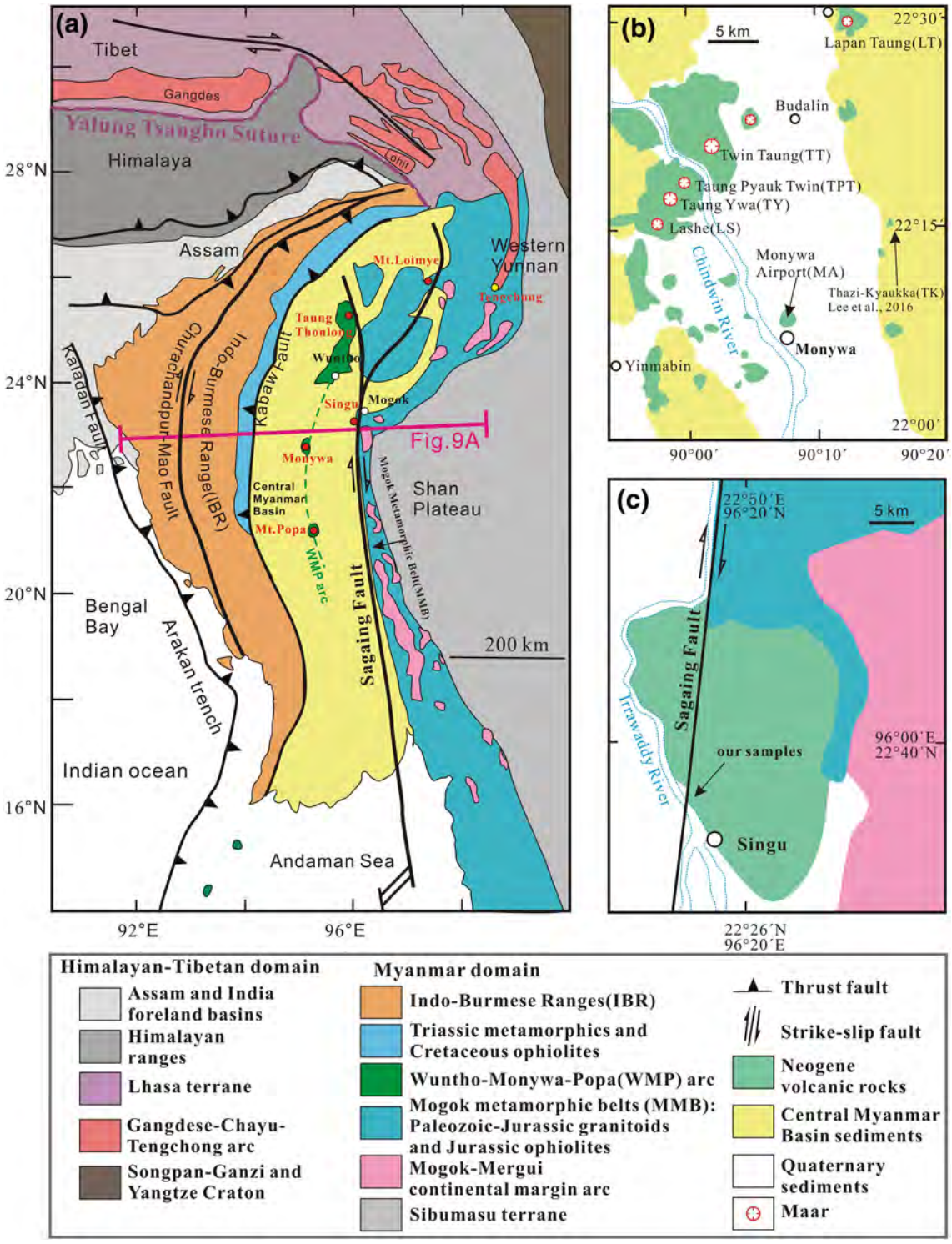

Figure 2. (a) Schematic map of the eastern Himalayan syntaxis and central Myanmar (after Licht et al., 2018). The approximate axis of the Wuntho-Monywa-Popa (WMP) arc is shown by a green dashed line. The red line indicates the location of the cross section in Figure 9a. (b and c) Simplified geological maps for the Monywa and Singu volcanic centers, respectively.

West of the Sagaing Fault, the Central Myanmar Basins comprise two N-S trending troughs of the western forearc basin and eastern backarc basin (Cai et al., 2019; Licht et al., 2018; Wang et al., 2014), which are divided by the WMP arc (e.g., Li et al., 2020; Mitchell et al., 2012; Figure 2a). The WMP arc may correlate with the Gangdese arc of southern Tibet linked by the Lohit batholith though pre-110 Ma magmatic records have not been reported within the WMP arc (Li et al., 2020; Lin et al., 2019; Mitchell et al., 2012). The forearc region was an Andean-type subduction margin and fed by the denudation of the Wuntho-Popa magmatic arc to the east until ~39 Ma (Cai et al., 2019; Licht et al., 2018; Wang et al., 2014). Since then, both forearc and backarc basins (Figure 2a) have transitioned to pull-apart basins as a result of onset of the strike-slip deformation on the highly oblique subduction margin (Licht et al., 2018; Morley & Arboit, 2019); the main depositional centers in central Myanmar have shifted southward, and thus, the modern low plains have developed (Licht et al., 2018).

Five Quaternary volcanic centers (Figure 2a), including Mt. Loimye, Taung Thonlong, Singu, Monywa and Mount Popa from north to south, are sporadically distributed along the midline of the central Myanmar basins, and some of them are very young (Bender, 1983; Bertrand et al., 1998; Lee et al., 2016; Maury et al., 2004; Stephenson & Marshall, 1984). The Monywa and Singu volcanic areas are reported on here (Figures 2b and 2c). In Monywa, most samples were collected from Lashe, Taung Ywa, Twin Pyauk Taung, Twin Taung, and Lapan Taung, which are distributed along a NE-SW line (Figure 2b). It is noteworthy that very coarse grained ultramafic and gabbroic cumulates were identified only in Twin Taung volcanic rocks (Maury et al., 2004). Volcanic rocks near the Monywa Airport were also collected in this study. Shoshonitic basalts from Thazi and Kyaukka were reported by Lee et al. (2016). The Singu basaltic flows, north of Mandalay, form a 100-km^2 plateau that has been subsequently offset by the dextral motion of the Sagaing Fault (Figure 2c; Bertrand et al., 1998). The Lashe basalts of the Monywa area have phenocrysts of fine-grained olivine and plagioclase (Figure 3a). The basaltic rocks from Taung Ywa, Twin Pyauk Taung, Lapan Taung, and Monywa Airport usually have ~5 vol.% olivine phenocryst scattered in the groundmass (Figure 3b). Alternatively, the Twin Taung volcanic rocks have more than 15 vol.% coarse-grained phenocrysts of olivine, clinopyroxene, hornblende, and phlogopite and fine-grained plagioclase (Figure 3c). The Singu tranchybasalts usually have vesicular textures and microphenocrysts of olivine and needle-like plagioclase (Figure 3d). The K-Ar ages of Twin Taung and Singu volcanics have been documented by Maury et al. (2004) and Bertrand et al. (1998) and yielded 0.24 and 0.25–0.46 Ma, respectively.

3. Methods

Whole-rock major element concentrations were determined using an AXIOS X-ray fluorescence spectrometer at the Institute of Geology and Geophysics, Chinese Academy of Sciences; loss on ignition (LOI) was measured after 1-hr baking at 1000°C for each sample. Analytical uncertainties are generally better than ±1% for all major elements. Whole-rock trace elements (including rare earth element, REE) were determined in solution mode using a Thermo quadrupole inductively coupled plasma mass spectrometer at the Institute of Tibetan Plateau Research, Chinese Academy of Sciences (ITPCAS). BHVO-1 and BCR-1 standards were used to monitor the accuracy and reproducibility with a relative standard deviation of better than 5%. Whole-rock Sr and Nd isotopes were measured on a Nu Plasma II multicollector inductively coupled plasma mass spectrometer at ITPCAS; methodologies followed Wang et al. (2017). Samples for Sr and Nd isotopic analysis were digested in an acidic mixture of HF-HNO_3 in Teflon bombs at 150°C for 48 hr. Sr and Nd were separated in cation exchange columns containing AG50W-X4 resin and TODGA resin, respectively. Measured $^{87}Sr/^{86}Sr$ and $^{143}Nd/^{144}Nd$ ratios were normalized to $^{146}Nd/^{144}Nd = 0.7219$ and $^{86}Sr/^{88}Sr = 0.1194$ for mass fractionation corrections. The NBS-987 and JNdi-1 international standards were used to assess instrument stability during data collection. The total procedural blanks were 70 pg for Nd and 300 pg for Sr, which is negligible considering the measured Nd-Sr concentrations of the samples. During the course of this study, the mean $^{87}Sr/^{86}Sr$ value for NBS987 was 0.710240 ± 9 ($n = 8$, 2σ) and the mean $^{143}Nd/^{144}Nd$ for JNd_i-1 was 0.512120 ± 5 ($n = 8$, 2σ), respectively. In addition, the BCR-2 external standard yielded $^{87}Sr/^{86}Sr = 0.705007 \pm 9$ and $^{143}Nd/^{144}Nd = 0.512631 \pm 6$ ($n = 4$). For routine analyses, the 2σ analytical errors are usually <0.000020 for $^{87}Sr/^{86}Sr$ and <0.000010 for $^{143}Nd/^{144}Nd$.

Using the Carius tube method for Re-Os isotope analysis, about 2 g of whole-rock powder spiked with appropriate amounts of ^{185}Re and ^{190}Os, was digested with 2 ml concentrated HCl and 8 ml HNO_3 at 230°C for 72 hr. Os was

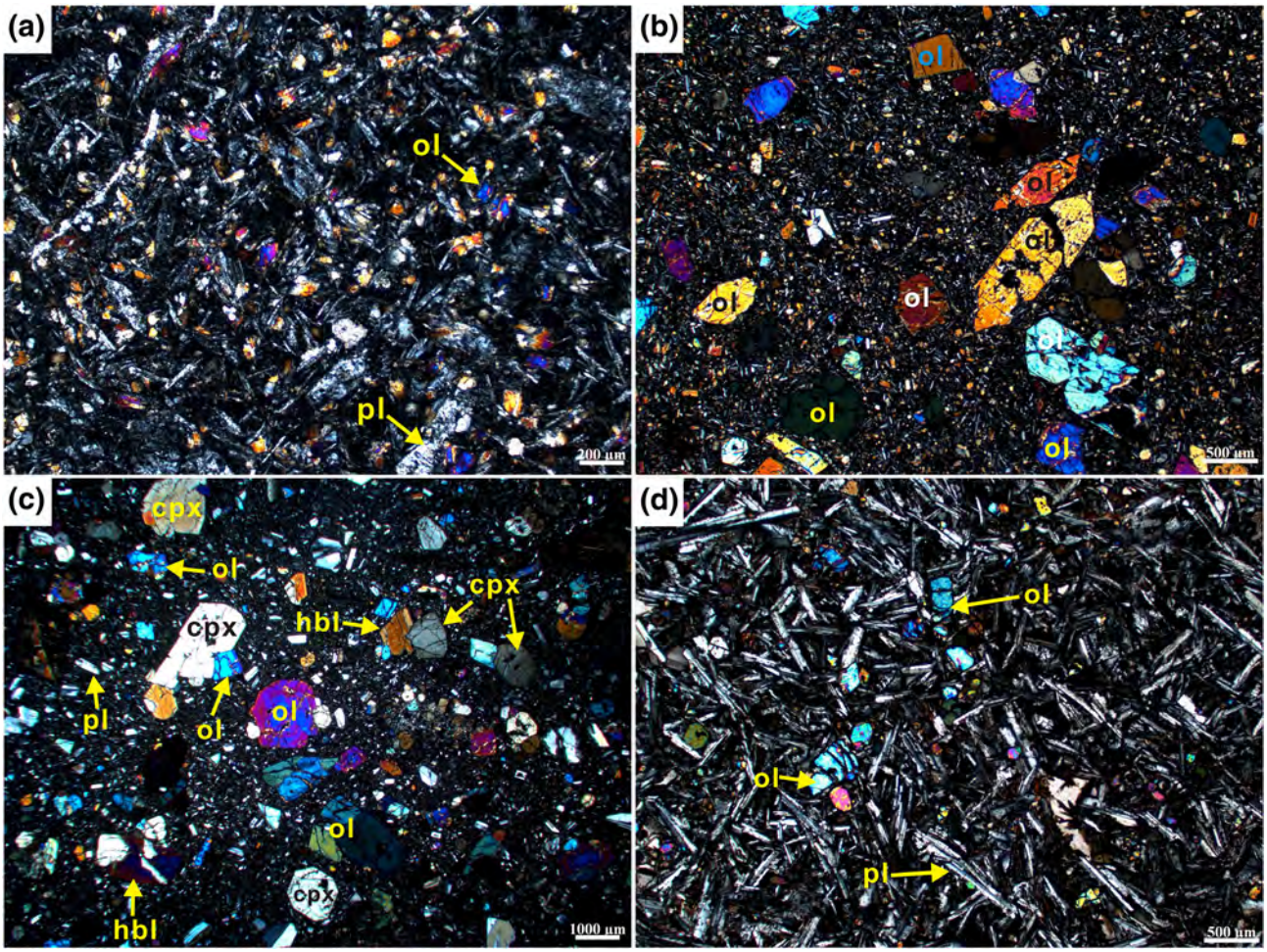

Figure 3. Cross-polarized light photomicrographs of Quaternary Myanmar volcanic rocks. (a) Low-K tholeiitic rocks in Lashe (16TPT13), (b) medium-K calc-alkaline rocks in Twin Pyauk Taung (16TPT01A), (c) high-K to shoshonitic rocks in Twin Taung (16TD01E), and (d) OIB-like rocks in Singu (15M147C); ol, olivine; cpx, clinopyroxene; hbl, hornblende; pl, plagioclase.

distilled at 110 °C for 1 hr; meanwhile, OsO_4 was absorbed using HBr solution and then further purified via microdistillation method (Birck et al., 1997). After the distillation of Os, the remaining sample was treated with HF and 1.2 M HCl solution (Ishikawa et al., 2014). Then Re was extracted and purified by using Rare Earth (RE) resin chromatographic separation. Further details for both Re and Os chemical and analytical techniques can be found in Huang et al. (2018). Os isotopic compositions were determined with a Thermo-Fisher TRITON Plus thermal ionization mass spectrometer operated in the negative ion mode (N-TIMS, Creaser et al., 1991; Völkening et al., 1991) at the State Key Laboratory of Continental Dynamics, Department of Geology, Northwest University, China. Purified Os was loaded onto platinum filaments with Ba $(OH)_2$ as an ion emitter. The OsO_3^- signal was enhanced by the introduction of O_2 gas to the source during the running. The measured Os isotopic ratios were corrected for mass fractionation using $^{192}Os/^{188}Os = 3.08271$. The in-run precisions for Os isotopic measurements were better than 0.2% (2RSE) for all the samples. Re contents were measured using multicollector inductively coupled plasma mass spectrometer at ITPCAS. The in-run precisions for Re concentrations ranged from 0.6% to 6%. The total procedural Os blanks were between 0.5 and 2.0 pg with $^{187}Os/^{188}Os$ of 0.116 ± 0.014 ($n = 10$). For a sample size of 2 g, the blank/sample ratio was usually 0.25–1.0 pg Os/g powder. Total procedural Re blanks were between 0.7 and 1.6 pg. Re concentrations and Os isotopic compositions presented in supporting information Table S1 were not corrected for the blank contribution. Blanks of this size have some effects on the Os isotopic compositions of the smallest samples, but the conclusions of this study are not affected. During the course of this study, the WPR-1 standard yielded an average $^{187}Os/^{188}Os$ ratio of 0.14428 ± 0.00009 (2σ, $n = 2$), which is in good agreement with the previously reported values (Huang et al., 2018).

4. Results

Major and trace element data and Sr-, Nd-, and Os-isotopic compositions are presented in supporting information Table S1. Most of the samples yielded LOI < 2 wt.%, consistent with the freshness of these Quaternary volcanic cones; some rocks with LOI > 2 wt.% are associated with variable LILE concentrations (e.g., Na, K, Rb, Ba, and Sr). However, the $^{87}Sr/^{86}Sr$ did not scale with LOI, which supports a negligible effect of alteration on the Sr isotopic compositions, suggesting that our data are robust and can be used to interpret the magmatic origin of the volcanic rocks.

The Singu and Twin Taung volcanic rocks are within the alkaline field (Figure 4a) and are also enriched in potassium (K_2O = 2–4 wt.%; Figure 4b). The Singu trachybasalts and basaltic trachyandesites exhibit higher TiO_2 (~2 wt.%) than the other volcanic rocks (Figure 4c). Regarding the subalkaline samples shown in Figure 4b, the Lashe basalts are tholeiitic with relatively low K_2O (down to 0.2 wt.%), whereas the Taung Pyauk Twin, Taung Ywa, Lapan Taung, and Monywa Airport basalts are calc-alkaline with medium K_2O (0.5–1 wt.%). Most of the medium-K rocks from Monywa have high MgO (8 to 12 wt.%), Cr (258–598 ppm, Figure 4d), and Ni (75–209 ppm, Figure 4e) compositions suggesting near primary melt compositions. The low-K basalts from Monywa show relatively low MgO (6 to 7 wt.%), Cr (120–293 ppm), and Ni (50–88 ppm). The high-K to shoshonitic rocks from Monywa exhibit a wide range of MgO (4.5 to 13 wt.%), Cr (11–607 ppm), and Ni (18–220 ppm). The Singu rocks have relatively low MgO (4.7 to 6.9 wt.%), Cr (83–171 ppm), and Ni (79–108 ppm). All the rocks studied here are basaltic with SiO_2 < 52 wt.% and have a wide range of CaO concentrations (Figure 4f).

On the chondrite-normalized REE diagram (Figure 5a), the Lashe low-K tholeiitic basalts display relatively flat REE patterns, whereas the other rocks show strongly enriched light rare earth elements (LREE) patterns. The primitive mantle-normalized multiple element plots (Figure 5b) illustrate the very different geochemical signatures of the Singu rocks with respect to the Monywa rocks studied here. All the Monywa rocks are characterized by their high field strength element (Nb-Ta, Zr-Hf, and Ti) depletions with respect to adjacent incompatible elements, which is usually understood to imply the presence of a subduction-modified component in the mantle source and/or crustal contamination (e.g., Aldanmaz et al., 2000). The Singu samples display totally different patterns with slightly positive anomalies in high field strength element (Figure 5d), which is generally considered typical of intraplate or oceanic island basalts (OIB; Pearce, 2008). Furthermore, on the highly discriminant trinary plotting diagrams, the Singu tranchybasalts all plot within the intraplate field, whereas the Monywa rocks studied here plot within the volcanic arc field (Figures 5c and 5d).

The initial Sr-Nd-Os isotope compositions for all the rocks are illustrated in Figure 6. The Singu rocks exhibit higher $^{87}Sr/^{86}Sr_i$ (0.7056 to 0.7064) but lower εNd_i (+0.8 to +1.6) values than the Monywa rocks studied here ($^{87}Sr/^{86}Sr_i$ = 0.7043 to 0.7047; εNd_i = +2.3 to +4.7; Figure 6a). Both the Monywa and Singu rocks have the very low Os concentrations (2 to 22 ppt) but extremely high and variable $^{187}Os/^{188}Os_i$ ratios (0.1498 to 0.3824, Figure 6d).

5. Discussion

5.1. Magmatic Sources and Mantle Flow

Mantle-derived primary magmas have high MgO, Ni(>400 ppm), and Cr(>1,000 ppm) (Wilson, 1989). The Monywa high MgO (>9 wt.%) samples exhibit positive correlations between Ni and MgO and negative correlations between CaO and MgO (Figures 4e and 4f), indicative of early fractionation crystallization of olivine. The Monywa and Singu low MgO rocks (<9 wt.%) show positive correlations between CaO and MgO (Figure 4f), suggesting primary fractionation crystallization of clinopyroxene and plagioclase. However, the distinct REE and trace element patterns (Figures 5a and 5b) and the diagnostic diagrams (Figures 5c and 5d) suggest controls on the final rock compositions beyond a simple magmatic fractionation process. The negative correlations between MgO and εNd_i are weak for the Monywa rocks, but crustal contamination cannot be easily excluded (Figure 6b). Such contamination requires either crustal assimilation during magma ascent or input of the subducted sediments during mantle melting (Plank & Langmuir, 1998). Earlier studies suggested that the Monywa rocks underwent little crustal assimilation but were significantly modified by subducted fluids/sediments during mantle wedge melting (Lee

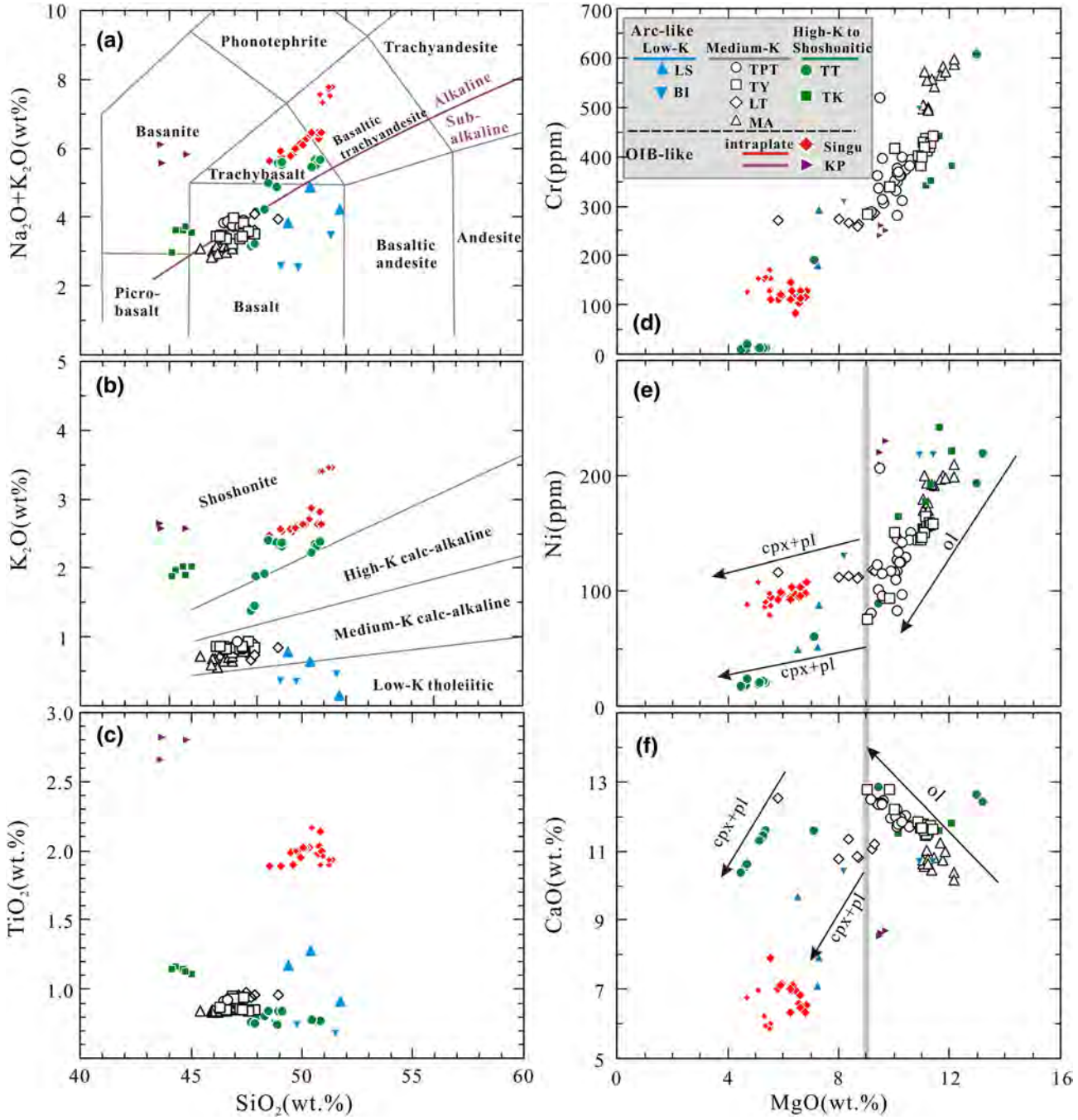

Figure 4. (a) Total alkalis vs. SiO_2 diagram (Le Bas et al., 1986), (b) K_2O vs. SiO_2 (Peccerillo & Taylor, 1976); (c) TiO_2 vs. SiO_2, (d) Cr vs. MgO, (e) Ni vs. MgO, (f) CaO vs. MgO. LS: Lashe; BI: Barrel Island (Chandrasekharam et al., 2009; Luhr & Haldar, 2006; MgO > 8 wt.%); TPT: Taung Pyauk Twin; TY: Taung Ywa; LT: Lapan Taung; MA: Monywa Airport; TT: Twin Taung; TK: Thai-Kyaukka (Lee et al., 2016); Singu (Lee et al., 2016, and this study); KP: Khorat Plateau, Thailand (An et al., 2017; MgO > 8 wt.%). Larger symbols are data from this study, and smaller symbols are data from the literature; ol, olivine; cpx, clinopyroxene; pl, plagioclase.

et al., 2016; Maury et al., 2004). All the Monywa rocks, including the most evolved Twin Taung suite, show little correlation between $^{87}Sr/^{86}Sr_i$ and MgO (Figure 6c), which also argue against extensive crustal assimilation. The Singu OIB-like rocks were thought to be significantly contaminated by ancient basement of the Sibumasu terrane due to their higher $^{87}Sr/^{86}Sr_i$ and lower εNd_i values (e.g., Lee et al., 2016). However, the Nb/U ratios (36 to 87, Table S1) of the Singu rocks are significantly higher than that of continental crust (9 ± 3, Rudnick, 2003), which can rule out significant crustal contamination. In

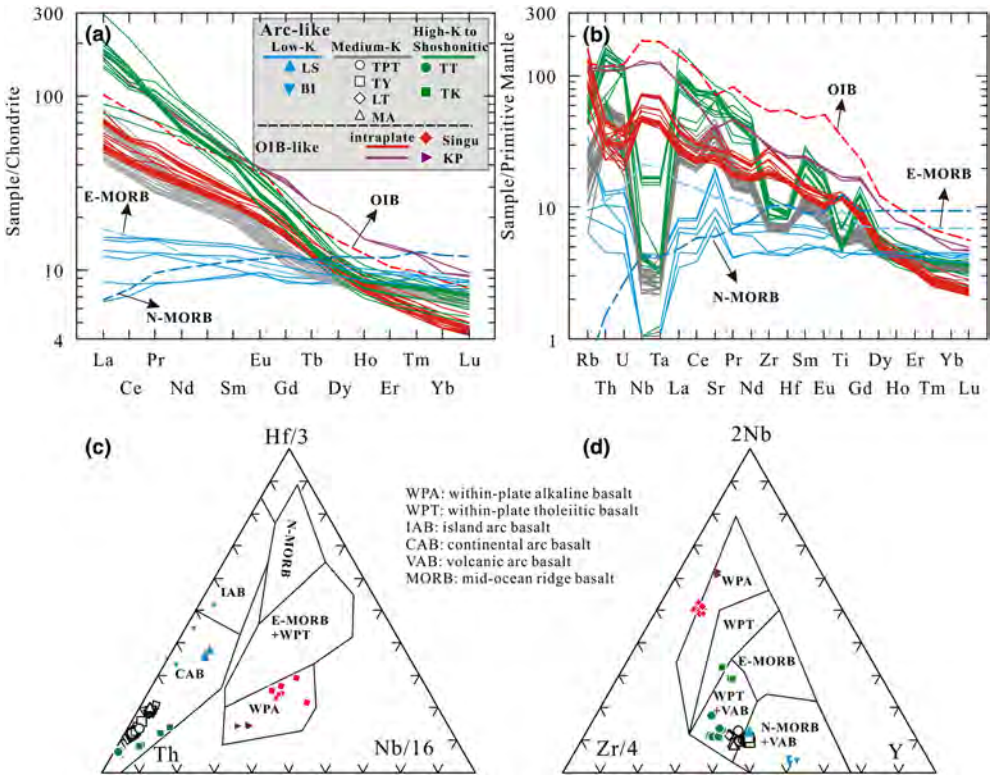

Figure 5. (a) Chondrite-normalized REE patterns, (b) primitive mantle-normalized trace element diagram, (c) Hf-Th-Nb (Wood, 1980), and (d) Nb-Zr-Y (Meschede, 1986) for the Quaternary Myanmar volcanic rocks. Data of chondrite, primitive mantle, OIB, N-MORB, and E-MORB are from Sun and McDonough (1989).

addition, their uniform REE and trace element patterns also argue against extensive crustal assimilation (Figures 4g and 4h).

Os isotopic ratios of basalts are particularly sensitive to crustal contamination, which generates isotopic ratios that are remarkably distinct from those of their mantle sources (Shirey & Walker, 1998). Even minor amounts of crustal contamination have the potential to significantly alter the Os isotopic compositions of Os-poor basalts (McBride et al., 2001; Reisberg et al., 1993). The rough negative correlations between Os concentrations and $^{187}Os/^{188}Os_i$ ratios for the Myanmar basalts and their higher $^{187}Os/^{188}Os_i$ values than those of the mantle wedge peridotites are indicative of crustal contamination (Figure 6d). The Monywa and Singu basalts have positive correlations between MgO and Os contents (Figure 6e), suggesting that their Os concentrations were also likely to be strongly affected by fractional crystallization. It is thus likely that the basaltic magmas approached the lower continental crust with a wide range of Os concentrations due to progressive magmatic differentiation. To roughly estimate the amounts of contamination needed to produce the observed $^{187}Os/^{188}Os$ ratios, we used a simple binary mixing model (Figure 6f). We assumed the parent magma of the Myanmar basalts to have varying Os concentrations (50 to 1 ppt, gray solid lines) with a mantle-like $^{187}Os/^{188}Os$ ratio of 0.128, contaminated with $^{187}Os/^{188}Os$ of 0.8 and Os concentrations of 49 ppt taken as being representative of the continental lower crust (Saal et al., 1998). The modeling results suggest that the addition of less than 4% of lower crust can replicate the observed covariation between $^{187}Os/^{188}Os$ and 1/Os. Therefore, the Os isotopic compositions of the Os-poor Monywa and Singu basalts mainly reflect minor crustal contamination rather than their mantle source heterogeneity.

However, addition of minor amounts (0.5–4%, Figure 6f) of lower crust would not have much effect on incompatible elements and Sr-Nd isotopic ratios for the Monywa and Singu volcanic rocks. For example, if the ancient lower crust was assumed to have Nd concentration of 20 ppm and Sr concentration of 320 ppm (Rudnick, 2003) with $^{143}Nd/^{144}Nd$ of 0.5118 and $^{87}Sr/^{86}Sr$ of 0.74, the maximum (4%) contamination of lower crust only shifts the $^{143}Nd/^{144}Nd$ by ~0.000016 (about 0.3 εNd unit) and $^{87}Sr/^{86}Sr$ by ~0.00002

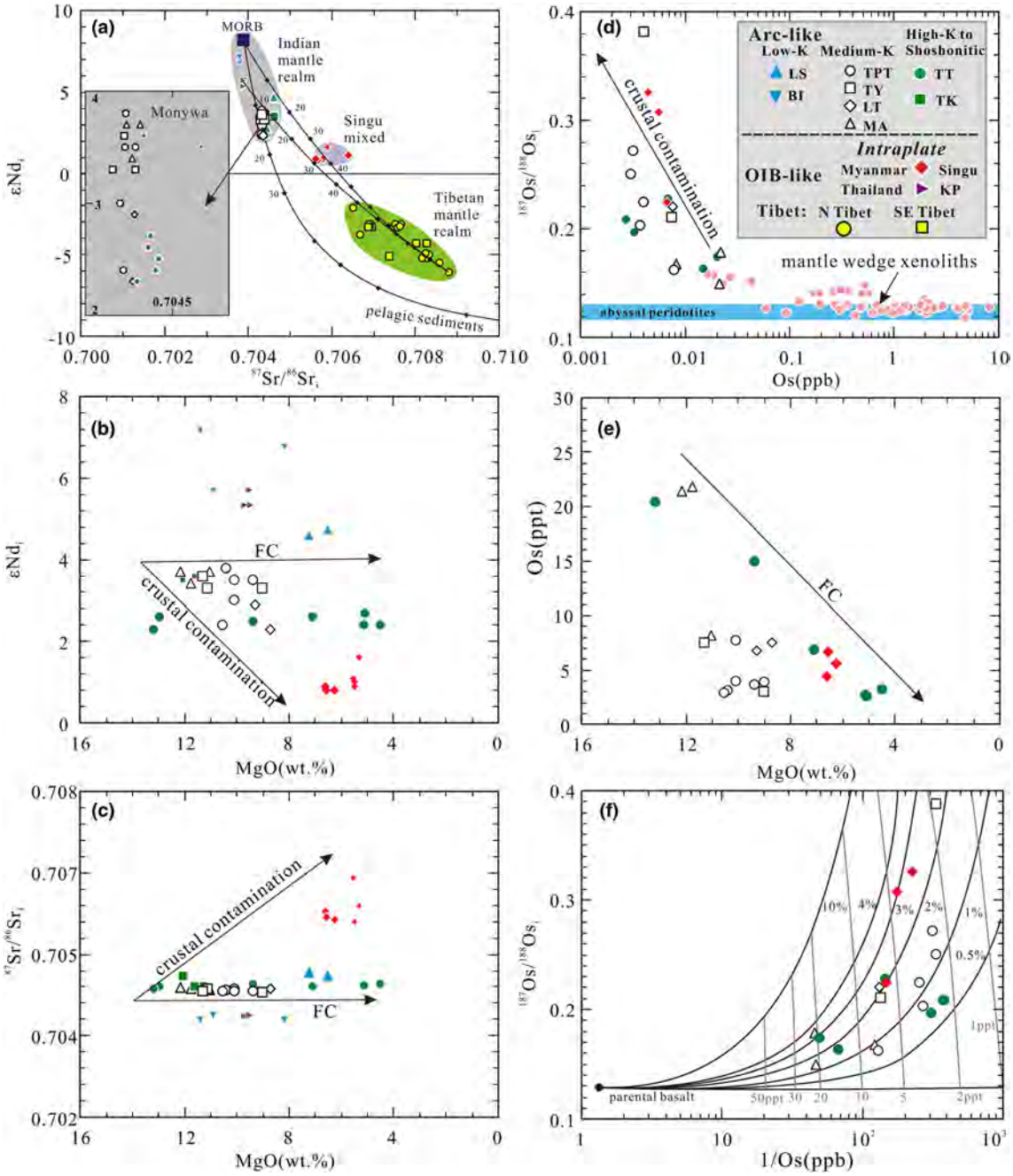

Figure 6. (a) $^{87}Sr/^{86}Sr_i$ vs. εNd_i; Sr- and Nd-isotopic data of the northern Tibetan primitive lavas (MgO > 8 wt.%) are from Guo et al. (2006) and Yang (2011) and SE Tibetan lavas of Tengchong from Tian et al. (2018) and Zhou et al. (2011). Data for Indian Mid-Oceanic Ridge Basalts (MORB) and pelagic sediments are from Mahoney et al. (1989) and Plank and Langmuir (1998), respectively. The end members for the binary mixing curves include the Indian MORB (Sr = 207 ppm, Nd = 12 ppm, $^{87}Sr/^{86}Sr = 0.7039$, and $^{143}Nd/^{144}Nd = 0.51305$), pelagic sediment (Sr = 302 ppm, Nd = 23.6 ppm, $^{87}Sr/^{86}Sr = 0.71236$, and $^{143}Nd/^{144}Nd = 0.51211$), Tibetan shoshonite (Sr = 1,068 ppm, Nd = 80 ppm, $^{87}Sr/^{86}Sr = 0.7088$, and $^{143}Nd/^{144}Nd = 0.51233$), and Khorat Plateau OIB rock (Sr = 621 ppm, Nd = 50 ppm, $^{87}Sr/^{86}Sr = 0.7039$, and $^{143}Nd/^{144}Nd = 0.51293$). (b) MgO vs. εNd_i $^{87}Sr/^{86}Sr_i$, (c) MgO vs. $^{87}Sr/^{86}Sr_i$, and (d) Os vs. $^{187}Os/^{188}Os_i$; Os compositions for mantle wedge xenoliths in subduction zones are from literature data (Liu et al., 2018, and references therein). (e) MgO vs. Os and (f) 1/Os vs. $^{187}Os/^{188}Os_i$ diagram showing the binary mixing model between the Myanmar parent basalts with varying Os contents (Os = 50 to 1 ppt; $^{187}Os/^{188}Os = 0.128$; gray solid lines) and lower continental crust (Os = 49 ppt; $^{187}Os/^{188}Os = 0.8$, Saal et al., 1998).

for the Monywa and Singu rocks. Therefore, the Sr-Nd isotopic compositions mainly represent those of their mantle source characteristics beneath Myanmar.

Two distinct groups emerge from the geochemical characteristics and spatial distributions presented above: the Monywa arc-like and the Singu OIB-like (Figure 5). The Monywa arc-like rocks are distinguished from the Singu OIB-like rocks by their negative HSFE anomalies on the multiple incompatible element plot (Figure 5b) as well as lower TiO_2 (Figure 4c). The Monywa arc-like rocks plot in three different compositional fields: low-K tholeiitic, medium-K, and high-K to shoshonitic rocks (Figure 4b). The Lashe basaltic rocks are tholeiitic with low K_2O, have relatively flat REE patterns, and exhibit slightly negative Nb, Ta anomalies (Figure 5b). These low-K tholeiitic basalts with MORB-like REE patterns, also cropping out in the Barren Island (Figure 1; Chandrasekharam et al., 2009; Luhr & Haldar, 2006), were generated by asthenosphere decompression with slightly more mass transfer from the subducting plate. The medium-K calc-alkaline basalts are more abundant in this study and include Taung Pyauk Twin, Taung Ywa, Lapan Taung, and Monywa Airport, which have LREE enriched patterns (Figure 5a). The Twin Taung rocks are high-K to shoshonitic and are highly enriched in LREE, similar to those from Thai-Kyaukka (Figure 5b; Lee et al., 2016). The Singu OIB-like rocks are also high in K_2O (Figure 4b) and show slightly positive HSFE anomalies; this is similar to the late Cenozoic OIB-like basalts in Khroat Plateau, Thailand (Figures 1 and 5; An et al., 2017). However, the Singu rocks exhibit Sr-Nd isotopic signatures that are distinct from the Monywa arc-like rocks and the Khroat Plateau OIB-like rocks (Figure 6a).

Basaltic samples from the Monywa and Singu volcanic centers on the Th/Yb vs. Nb/Yb diagram help delineate the variable mantle contributions (Figure 7a). The Th/Nb ratios are almost independent of typical fractional crystallization and/or partial melting lines and thus are interpreted to indicate mantle source heterogeneity (Pearce, 2008). Basaltic magmas derived from the mantle asthenosphere, plume asthenosphere or mantle lithosphere enriched by small-degree melts from the asthenosphere, typically plot within or close to a diagonal mantle array defined by constant Th/Nb ratios (Figure 7a; Pearce, 2008). A source region metasomatized by subduction components with higher Th/Nb ratios, however, can results in an enrichment of Th with respect to Nb (Pearce, 2008). All the Monywa rocks exhibit compositions that are consistent with the incorporation of crustal inputs during subduction, typical of volcanic arc basalts (Figure 7a). Crustal inputs during subduction include both sediment melts and slab fluids and are typically observed in arc magmas (Figure 7b). In contrast, the Singu rocks show affinities with oceanic island basalts, indicative of asthenosphere melts without subduction input (Figure 7a).

The Th/Yb ratios increase as the Monywa arc-like rocks switch from the low-K tholeiitic to the medium-K calc-alkaline and to the shoshonitic fields (Figure 7a); this could be associated with decreasing degrees of partial melting at variable depths. We use the water-sensitive geobarometer of Lee, Chung, et al. (2009) to set new constraints on the temperatures and depths of magma generation for the Monywa magmas. The *P-T* conditions are estimated for the last melt in equilibrium with the mantle source or averaged *P-T* estimates of a polybaric melt that pooled along the magmatic conduits (Kelley et al., 2010). We used primitive magmas (MgO > 9 wt.%; Figures 4e and 4f) to ensure only olivine crystallized along their liquid line of descent. We considered that the primary melts were in equilibrium with a depleted mantle with a forsterite content of Fo_{90} as in Kelley et al. (2010) and Lee, Chung, et al. (2009). Unfortunately, the preeruptive water contents of Monywa arc basalts are not known. Assuming H_2O of 4 wt.% and a Fe^{3+}/Fe_T ratio of 0.2 for calculation, the low-K magmas recorded shallower and cooler *P-T* conditions for mantle-melt equilibrium conditions (Figure 7d; 1,182–1,195°C; 0.9 GPa) than those of the medium-K magmas (1,240–1,259°C; 1.4–1.6 GPa). The high-K to shoshonitic magmas in Thai-Kyaukka (1,263–1,276°C; 1.7–1.8 GPa) recorded deeper and hotter *P-T* conditions than those of Twin Taung magmas (1,209–1,213 °C; 1.2 GPa). The OIB-like Singu magma *P-T* conditions were not constrained due to their low MgO (<7 wt.%), but the Khorat Plateau OIB magmas had much deeper and hotter mantle melting conditions (1,344–1,350 °C; 2.6–2.7 GPa) than the other rocks reported here. Our new *P-T* estimates (Figure 7d) indicate that melting depths increase as K_2O increases; this is in accordance with the covariations between $(Gd/Yb)_N$ and $(Dy/Yb)_N$ (Figure 7c). The $(Dy/Yb)_N$ ratios do correlate positively with $(Gd/Yb)_N$ ratios; that is, the steepest REE patterns are associated with the highest K_2O (Figure 7c). The $(Dy/Yb)_N$ values of the Lashe low-K tholeiitic rocks are slightly higher than those of MORB rocks, suggesting mantle melting in the spinel stability field. The Monywa high-K to shoshonitic rocks, like the Singu OIB-like volcanic rocks, have the highest $(Dy/Yb)_N$ values,

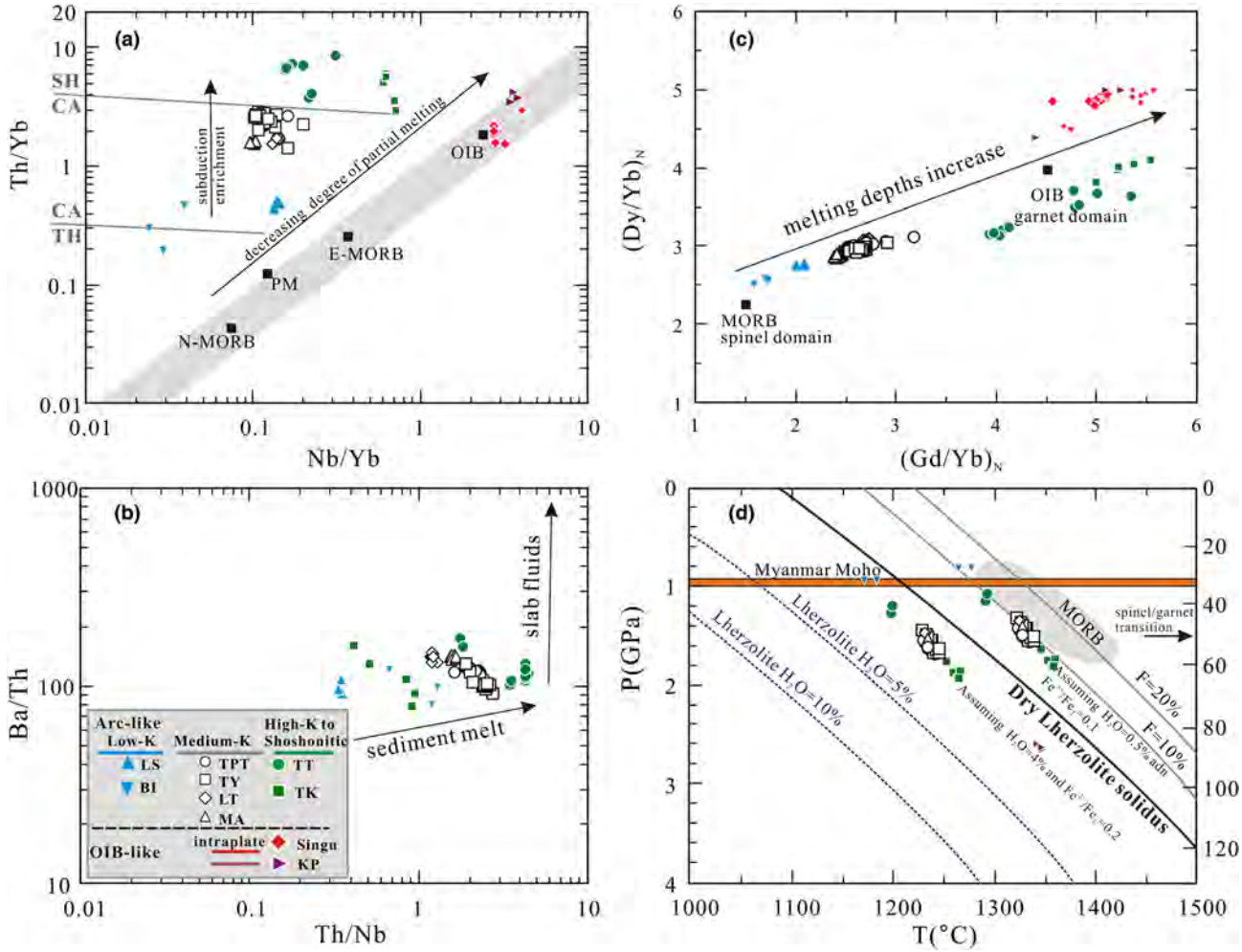

Figure 7. (a) Nb/Yb vs. Th/Yb (Pearce, 2008); (b) Ba/Th vs. Th/Nb; (c) $(Gd/Yb)_N$ vs. $(Dy/Yb)_N$, elevated $(Gd/Yb)_N$ and $(Dy/Yb)_N$ ratios indicate presence of garnet in mantle source; and (d) pressure and temperature of mantle-melt equilibrium for the primitive arc basalts in Monywa (Lee, Luffi, et al., 2009). Only basalts with >9 wt.% were used to ensure that they only crystallized olivine along their liquid line of descent (Figures 4e and 4f). Lherzolite solidi for varying water contents are taken from Katz et al. (2003). Samples were estimated assuming 0.5 and 4 wt.% water in the melts and olivine-fractionation corrected up to Fo_{90} in equilibrium with a depleted mantle.

also indicating that garnet was present in the mantle source. The medium-K magmas show moderate $(Dy/Yb)_N$ values, which suggests melting in the spinel-garnet transition zone. In addition, most samples are plot on the ~10% melt fraction contour of a dry fertile lherzolite, which is the temperature and pressure at which fertile lherzolite would melt 10% (Figure 7f; Katz et al., 2003); assuming a source beneath Myanmar more refractory than the mantle source of MORB would yield a slightly higher solidus and lower melting degree. These volcanic rocks are thus interpreted to be the products of small degrees of mantle melting resulting in the small volume of Quaternary volcanic rocks observed in Myanmar.

Nd isotope ratios of the Monywa arc-like basalts are characterized by their positive εNd_i values (+4.7 to +2.3) indicating an isotopically depleted mantle source (Figure 6a). However, the Monywa arc-like basalts are less depleted than that of the Indian MORB, which is usually explained through the addition of pelagic sediments during subduction (Plank & Langmuir, 1998). Simple binary modeling suggests that the Monywa arc-like basalts resulted from input of 8–15% sediments if the Indian MORB-type depleted mantle was present beneath Myanmar. In contrast, the Singu OIB-like basalts have higher $^{87}Sr/^{86}Sr_i$ (0.7056 to 0.7064) but lower εNd_i (+0.8 to +1.6) values; these plot away from the binary mixing curve above and indicate a distinct and relatively isotopically enriched asthenospheric mantle. One simple explanation for the Singu Sr-Nd isotopic compositions is that the Singu magmas are a mixture of two distinct melts sourced from both

Indian-type and Tibetan-type asthenosphere (Figure 6a), considering the mantle geodynamic setting to be discussed below.

Subduction of the Indian plate beneath the Eurasian plate has governed the horizontal shortening and growth of the Tibetan Plateau (e.g., Yin & Harrison, 2000; Figure 1), and asthenospheric mantle flow in general responds to the India-Asia convergence (e.g., Jolivet et al., 2018). As a result of this convergence, Asian continental lithosphere has subducted southward beneath northern Tibet in the areas of the eastern Kunlun Fault (e.g., Zhao et al., 2011). Beneath Tibet, Indian continental lithosphere subducted as far as the western Kunlun Fault in the Pamir and the Bangong-Nujiang suture in central Tibet before plunging vertically into mantle (e.g., Replumaz et al., 2010; Shi et al., 2015; Zhao et al., 2010). These sinking slabs induce upwelling of asthenosphere, and the vertical movement of these upwelling zones would bring up relatively hot mantle and possibly produce melts through adiabatic decompression to induce both crust and mantle-derived volcanism as well as maintaining high elevations (Guo et al., 2006; Wang et al., 2016; Yang, 2011). This geometry suggests that the downwelling slabs created continuous barriers in the deep mantle, which would block lateral flow of mantle in upwelling zones. The spatial distribution of these downwelling and upwelling zones have been imaged by the *P* wave velocity models in central and SE Tibet (e.g., Lei & Zhao, 2016; Li et al., 2008; Replumaz et al., 2010). The northeastward motion of the Indian plate with respect to the Eurasian plate (e.g., Replumaz et al., 2010; Zhang et al., 2004) and the steeply dipping lithospheric barriers in the mantle may have induced southeastward flow the upwelling mantle zones (Lei & Zhao, 2016). The geometries of slabs subducting into the mantle beneath Asia, including intracontinental subduction in northern Tibet (Zhao et al., 2011), and the continued northward migration of India into Asia are responsible for the flow of sub-Tibetan asthenosphere toward the Burmese microplate (e.g., Jolivet et al., 2018). This mantle flow model is supported by the results of azimuthal anisotropy inferred from SKS splitting results (Figure 1; Kind & Yuan, 2010; Liu et al., 2019; Wang et al., 2008).

Crust and mantle kinematics are thought to be decoupled at ~26°N (Figure 1), where orientations of mantle flow suddenly change from N-S to W-E (Figure 1; Kind & Yuan, 2010; Liu et al., 2019; Wang et al., 2008). This flow in the mantle would push the SE Tibetan asthenosphere across the inactive branches of the Sagaing Fault and approach northern Myanmar (Figures 1 and 2). The highly oblique subduction of the Indian slab beneath Burmese microplate would have provided a steeply dipping lithospheric barrier in the mantle (Li et al., 2008; Pesicek et al., 2010) that hamper mantle flow from SE Tibet further west but rather facilitated southward movement (Figures 1 and 8). The southward mantle flow along mantle wedge was probably enhanced due to the highly oblique subduction (e.g., arc-parallel mantle flow in central America; Rabbel et al., 2011) and might be further accelerated by the upwelling of asthenosphere beneath the Andaman sea initiated at ~4 Ma in response to backarc extension (Raju et al., 2004). This southward mantle flow beneath Myanmar may have provided sufficient space for westward escape of asthenosphere from SE Tibet. The Singu OIB-like magmas are interpreted as binary mixing melts generated through melting of both the Indian-type depleted and Tibetan-type enriched mantle asthenosphere (Figure 6a), which would be consistent with this mantle flow hypothesis (Figure 1).

5.2. Cause of Melting

Conditions became suitable for melting in the mantle beneath Myanmar; however, the precise trigger for melting is unclear. At most "typical" subduction zones, mantle wedge melting is generally induced by fluid fluxing and decompression (e.g., Davies & Stevenson, 1992; Ducea, Paterson, & DeCelles, 2015; Ducea, Saleeby, & Bergantz, 2015). However, subduction beneath the Burmese microplate is highly oblique according to geophysical, geodetic, and geological data below. Tomographic images suggest an eastward subduction of a high velocity anomaly beneath the Indo-Burmese Ranges (Lei & Zhao, 2016; Li et al., 2008; Pesicek et al., 2010; Figure 9b), while the Burmese microplate is mechanically driven northward with the Indian plate (Ni et al., 1989). The state of stress inferred from earthquakes does not support eastward relative motion of the Indian plate but rather northward motion with respect to the Sunda plate (Kundu & Gahalaut, 2012; Rao & Kumar, 1999). Global positioning system results indicate that northward motion of the Indian plate relative to the Sunda plate is accommodated primarily by slip on the CM and Sagaing right-lateral strike-slip faults (Gahalaut et al., 2013; Maurin et al., 2010l). Pull-apart basins developed, and E-W shortening is dominantly produced by strain partitioning of the major right-lateral shearing deformation rather than thrusting (Licht et al., 2018; Maurin & Rangin, 2009; Morley & Arboit, 2019). These observations above indicate that

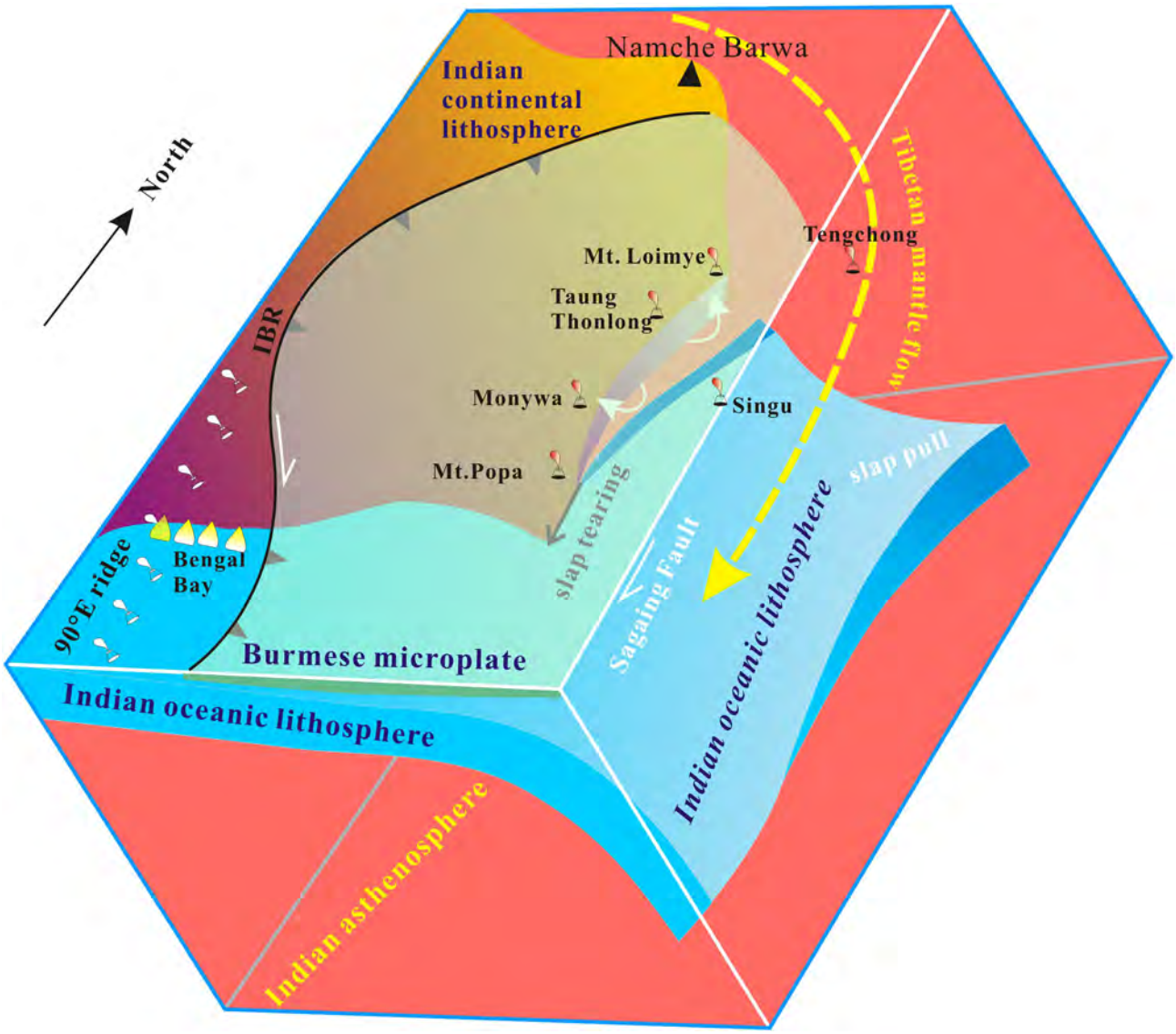

Figure 8. Southward slab tearing between Indian oceanic and continental lithosphere as the trigger for Quaternary volcanism in central Burmese microplate.

subduction beneath the Indo-Burmese Ranges has stopped and thus the E-W corner flow of convective mantle wedge is almost stagnated or "locked" as a result of this unusual highly oblique subduction (Figure 9a; MaCaffery, 1992). Therefore, both fluid-fluxing and decompression of peridotite within a typical mantle wedge would be suppressed or ineffective for causing melting beneath Myanmar. In this scenario, additional heating would be required to trigger mantle melting beneath Myanmar; however, the precise trigger for melting is unclear. Two distinct models for generation of the Quaternary volcanic rocks in Tengchong (Yunnan, China) and Myanmar were proposed: subduction of the 90°E ridge (Zhou et al., 2011) and the roll-back followed by slab "break-off" (Lee et al., 2016; Maury et al., 2004).

If the 90°E ridge model is considered, thick oceanic plateau would be more buoyant than the adjacent oceanic lithosphere and thus promote tearing of the down-going slab with possibly flatter subduction along the ~410 km discontinuity where the melts of the Tengchong volcanic rocks may have originated from (Zhou et al., 2011). However, much of the 90°E Ridge is probably covered by Bengal turbidites (Figure 1). The bathymetric expression of the 90°E Ridge can be observed on the floor of the Indian Ocean. Multichannel seismic studies indicate that the 90°E Ridge is present below the thick marine strata of the Bengal Fan between 15°N and 21°N (Rangin et al., 2013, Figure 7b; Sibuet et al., 2016, Figure 13). Furthermore, the 90°E Ridge as a result of the Kerguelen plume magmatism can be traced through the Rajmahal and

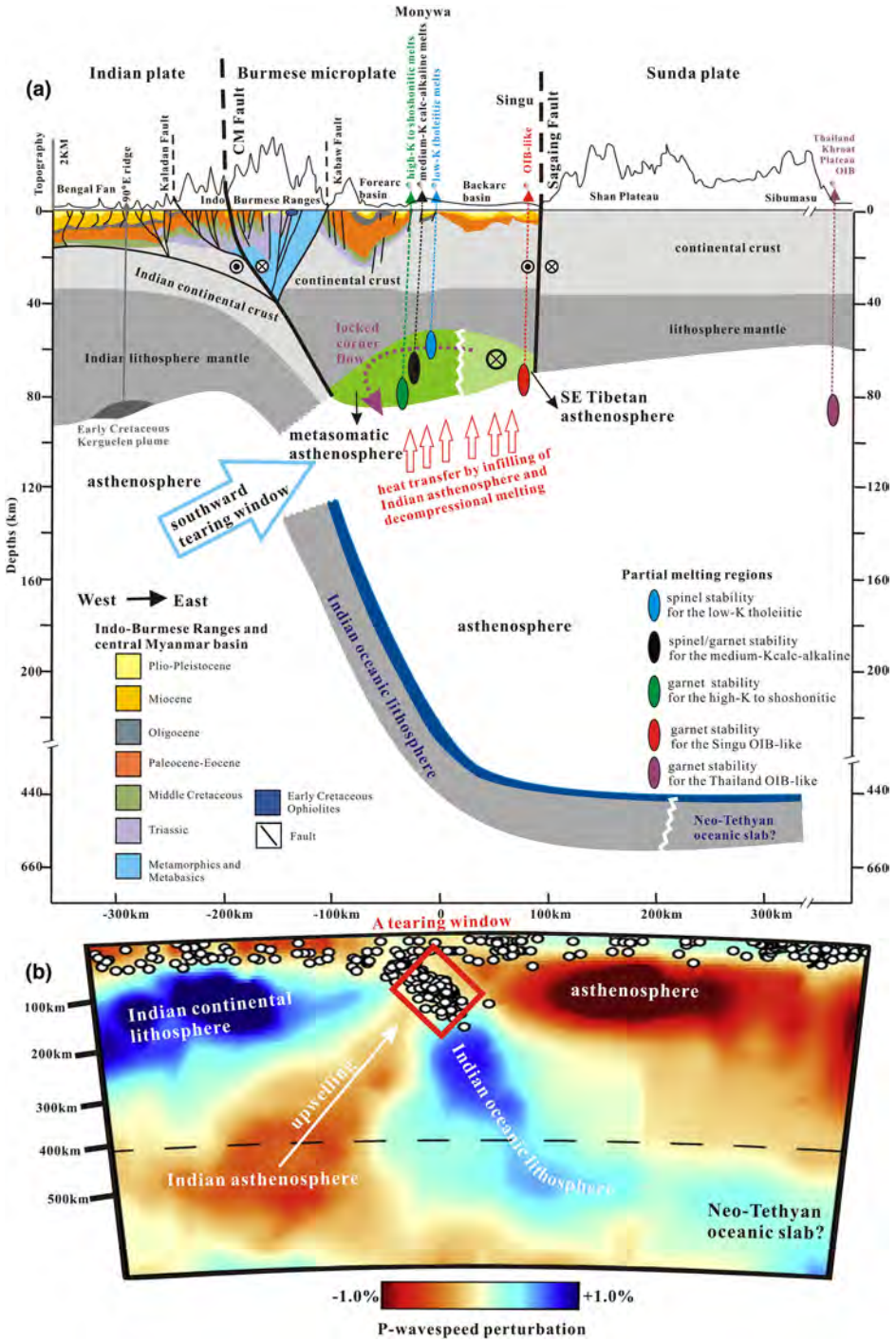

Figure 9. (a) Inferred tectonic setting and melting model for the central Myanmar quaternary volcanism (E-W section line shown in Figures 1 and 2). (b) Tomograhic image from Li et al. (2008); line of the section passes ~200 km north of the Monywa-Singu volcanic centers. In our opinion, this image indicates that the upwelling of the Indian asthenosphere is probably triggered by the slab detachment where the Indian oceanic lithosphere is being detached from the Indian continental lithosphere. Burmese microplate is wedged between India and Sunda plate and bounded by the CM and Sagaing right-lateral strike-slip faults (Gahalaut et al., 2013; Maurin et al., 2010). Earlier subducted Indian plate of oceanic and continental crust provided fluxing fluids that metasomatized the overriding Burmese mantle wedge. Exotic heat transferred by infilling of the Indian MORB asthenosphere through a window where the slab tearing occurred between Indian oceanic and continental lithosphere. As melting depths decrease, melting of the Burmese mantle wedge produced a variety of high-K to shoshonitic, medium-K calc-alkaline, and low-K tholeiitic basalts in Monywa. This upwelling asthenosphere experienced decompression melting and also heated the overlying asthenosphere layer, which flowed from SE Tibet. Mixing of these two isotopically distinct asthenospheric melts explains the origin of the Singu OIB-like rocks, which are in isotopic compositions distinct from those of the Khroat Plateau (Thailand) OIB basalts. Sedimentary strata of Indo-Burmese Wedge and central Myanmar basin are modified after Licht et al. (2018).

Sylhet Traps of northeastern India (Ingle et al., 2002) and Cuomei of the Tethyan Himalaya (e.g., Zhu et al., 2009). Therefore, there is little evidence supporting the notion that the 90°E Ridge has been subducted beyond the Burmese microplate for generating the Tengchong volcanic rocks because of orientation and long horizontal distance (~500 km) to the Kerguelen trace (Figure 1).

The westward directed rollback of the Indian oceanic lithosphere has been invoked as the primary causal of melting of the heterogeneous mantle beneath western Myanmar (Lee et al., 2016), although the spatiotemporal relationship between magmatism and rollback is unclear. Associations of scattered contemporaneous arc-like and OIB-like basalts have been ascribed to slab break-off and the formation of a slab window (Maury et al., 2004). However, it seems unlikely that slab break-off following rollback of the Indian slab occurred because the geodynamic processes usually result in broad mantle melting and a prolonged magmatic "flare-up" (e.g., 65–40 Ma Linzizong volcanic rocks and Gangdese batholiths, Chung et al., 2005; Lee, Luffi, et al., 2009; Zhu et al., 2015, and Neogene Mediterranean volcanic rocks, Dilek & Altunkaynak, 2009; Prelević et al., 2015). This contrasts with the observations that the volume of Quaternary volcanic rocks in central Myanmar is relatively low (Lee et al., 2016; Maury et al., 2004, and this study). Slab detachment is a migratory process, nucleating in one location and then migrating laterally (e.g., Yoshioka & Wortel, 1995). The tearing process may accelerate as the slab anchor force becomes focused over a decreasing area (Wortel & Spakman, 2000). The Burmese microplate is situated above a subduction transition from ocean to continent for the Indian plate (Figure 1). Therefore, we propose a southward propagating tear model in which the Indian oceanic lithosphere is being detached from its continental lithosphere (Figure 8) to generate the variable geochemical compositions of the Quaternary volcanic rocks described in this study (Figure 9a). This is consistent with the tomographic images indicating fast anomalies in the mantle dipping at 50–60° in the north near the eastern Himalayan syntaxis (Namche Barwa) and the subducted Indian lithosphere dipping at ~30° in the south near the Bay of Bengal area (Lei & Zhao, 2016; Li et al., 2008; Ni et al., 1989; Pesicek et al., 2010). In this zone between the Namche Barwa and the Bay of Bengal, we envision initiation of tearing along the subducting Indian plate and suggest that tearing may have started near the transition between oceanic and continental lithosphere in part due to the buoyant resistance to subduction of the latter (Figure 8). In this scenario the slab tearing facilitated some transfer of fresh Indian asthenosphere through the developing tear window (Figure 9). The transfer of this asthenosphere through the tearing window may have provided some additional heat to induce small degrees of mantle melting beneath the Burmese microplate.

We envision a scenario in which upwelling of the hot Indian asthenosphere (Figure 9b) would heat up both the previously metasomatized mantle wedge and the enriched asthenosphere layer sourced from the SE Tibet mantle flow (Figure 8). Partial melting of the Myanmar mantle wedge by the juxtaposition of relatively hot asthenosphere, previously metasomatized during earlier subduction of the Indian oceanic lithosphere, produced the Monywa low-K tholeiitic, medium-K calc-alkaline, and high-K to shoshonitic basalts at different depths. Partial melting of the isotopically enriched Tibetan asthenosphere mantle as well as decompression melting of the upwelling Indian depleted mantle at garnet stability fields produced the OIB-like Singu magmas with Sr-Nd isotope signatures mixed between the Indian and Tibetan mantle sources (Figure 6a). Slab tearing, unlike full detachment, can only provide limited heat (Niu, 2017), which would account for the low degrees melting, low magmatic productivity, and the narrow but linear distributions of basaltic rocks in central Myanmar (Lee et al., 2016; Maury et al., 2004; Stephenson & Marshall, 1984; Figure 2). This would explain the relatively small volume of Quaternary volcanism but would imply that mantle melting and thus volcanism could accelerate in the future. Furthermore, the redistribution and concentration of the slab pull force due to slab tearing (Figure 9a) are expected to affect the retreating migration of convergent plate margins, leading to an increase in arc curvature (Wortel & Spakman, 2000). This provides an alternative model to explain the westward convex of the Indo-Burmese Ranges (Figure 1), though this arc curvature may also be correlated with crustal flow from SE Tibet (e.g., Rangin et al., 2013).

6. Conclusions

The Burmese microplate, associated with Quaternary volcanism in a highly oblique subduction setting, is located above a transition from subduction of Indian oceanic lithosphere to continental lithosphere. According to our geochemical analysis, the Monywa volcanic rocks range from low-K tholeiitic to

medium-K calc-alkaline and to high-K and shoshonitic. These rocks display geochemical affinities to arc magmatism. In contrast, the Singu basaltic rocks are high in TiO_2 and display intraplate OIB-like geochemical signatures. These volcanic rocks have low Os concentrations but high $^{187}Os/^{186}Os_i$ ratios (0.1498 to 0.3824), indicating minor (<4%) crustal contamination. In central Myanmar, the Monywa arc-like rocks were probably generated by melting a small degree of previously metasomatized mantle wedge at depths ranging from the spinel to garnet stability fields. Distinct from a relatively depleted mantle melting for the Monywa arc-like rocks ($^{87}Sr/^{86}Sr_i = 0.7043$ to 0.7047; $\varepsilon Nd_i = +2.3$ to +4.7), the Singu OIB-like rocks exhibit lower εNd_i (+0.8 to +1.6) with higher $^{87}Sr/^{86}Sr_i$ (0.7056 to 0.7064). An overlying enriched asthenosphere layer derived from SE Tibetan mantle flow is one explanation that fits the geochemical observations of the Quaternary Singu volcanic rocks and the subducted plate geometries inferred from geophysical studies. The short-lived, low magmatic production of the Quaternary Myanmar volcanism as well as its nearly linear spatial distribution is a function of its deep geodynamics and positions above a slab tearing window where Indian oceanic lithosphere is being detached from continental lithosphere beneath Burmese microplate at mantle depths.

Data Availability Statement

Data for this paper can be accessed through the website (http://www.tpedatabase.cn).

Acknowledgments

We thank S. Q. Zhao and Q. Y. Guan for the help with isotopic analyses. This manuscript was strengthened by detailed comments from L. Reisberg, S. Guillot, and one anonymous reviewer and suggestions from Editor J. Blichert-Toft. This research was funded by the National Natural Science Foundation Project (Grants 41490613 and 41490615), the Strategic Priority Research Program of Chinese Academy of Sciences (XDA20070301), the Ministry of Science and Technology of China (Grant 2016YFC0600303), and the Second Tibetan Plateau Scientific Expedition and Research Program (STEP; Grant 2019QZKK0708). M. N. Ducea acknowledges support from U.S. National Science Foundation (Grant EAR 1725002) and the Romanian Executive Agency for Higher Education, Research, Development and Innovation Funding projects (Grants PN-III-P4-ID-PCE-2016-0127 and PN-III-P4-ID-PCCF-2016-0014).

References

Aldanmaz, E., Pearce, J. A., Thirlwall, M. F., & Mitchell, J. G. (2000). Petrogenetic evolution of late Cenozoic, post-collision volcanism in western Anatolia, Turkey. *Journal of Volcanology and Geothermal Research*, *102*(1), 67–95. https://doi.org/10.1016/S0377-0273(00)00182-7

An, A. R., Choi, S. H., Yu, Y., & Lee, D. C. (2017). Petrogenesis of late Cenozoic basaltic rocks from southern Vietnam. *Lithos*, *272*, 192–204. https://doi.org/10.1016/j.lithos.2016.12.008

Bender, F. (1983). Geology of Myanmar (pp. 1–293). Berlin: Borntraeger.

Bertrand, G., Rangin, C., Maury, R. C., Htun, H. M., Bellon, H., & Guillaud, J. P. (1998). Les basaltes de Singu (Myanmar): Nouvelles contraintes sur le taux de décrochement récent de la faille de Sagaing. *Comptes Rendus de l'Académie des Sciences - Series IIA - Earth and Planetary Science*, *327*(7), 479–484. https://doi.org/10.1016/S1251-8050(99)80076-7

Birck, J. L., Barman, M. R., & Capmas, F. (1997). Re-Os isotopic measurements at the femtomole level in natural samples. *Geostandards Newsletter*, *21*(1), 19–27. https://doi.org/10.1111/j.1751-908x.1997.tb00528.x

Cai, F., Ding, L., Zhang, Q., Orme, D. A., Wei, H., Li, J., et al. (2019). Initiation and evolution of forearc basins in the Central Myanmar Depression. *GSA Bulletin*, *132*, 1066–1082. https://doi.org/10.1130/B35301.1

Chandrasekharam, D., Santo, A. P., Capaccioni, B., Vaselli, O., Alam, M. A., Manetti, P., & Tassi, F. (2009). Volcanological and petrological evolution of Barren Island (Andaman Sea, Indian Ocean). *Journal of Asian Earth Sciences*, *35*, 469–487. https://doi.org/10.1016/j.jseaes.2009.02.010

Chung, S.-L., Chu, M.-F., Zhang, Y., Xie, Y., Lo, C.-H., Lee, T.-Y., et al. (2005). Tibetan tectonic evolution inferred from spatial and temporal variations in post-collisional magmatism. *Earth-Science Reviews*, *68*, 173–196. https://doi.org/10.1016/j.earscirev.2004.05.001

Creaser, R. A., Papanastassiou, D. A., & Wasserburg, G. J. (1991). Negative thermal ion mass spectrometry of osmium, rhenium and iridium. *Geochimica et Cosmochimica Acta*, *55*, 397–401. https://doi.org/10.1016/0016-7037(91)90427-7

Davies, J. H., & Stevenson, D. J. (1992). Physical model of source region of subduction zone volcanics. *Journal of Geophysical Research*, *97*(B2), 2037–2070. https://doi.org/10.1029/91jb02571

Davies, J. H., & von Blanckenburg, F. (1995). Slab breakoff: A model of lithosphere detachment and its test in the magmatism and deformation of collisional orogens. *Earth and Planetary Science Letters*, *129*(1-4), 85–102. https://doi.org/10.1016/0012-821x(94)00237-s

Dilek, Y., & Altunkaynak, Ş. (2009). Geochemical and temporal evolution of Cenozoic magmatism in western Turkey: Mantle response to collision, slab break-off, and lithospheric tearing in an orogenic belt. *Geological Society, London, Special Publications*, *311*, 213–233. https://doi.org/10.1144/SP311.8

Ducea, M. N. (2016). Understanding continental subduction: A work in progress. *Geology*, *44*, 239–240. https://doi.org/10.1130/focus032016.1

Ducea, M. N., Paterson, S. R., & DeCelles, P. G. (2015). High-volume magmatic events in subductionvsystems. *Elements*, *11*, 99–104. https://doi.org/10.2113/gselements.11.2.99

Ducea, M. N., Saleeby, J. B., & Bergantz, G. (2015). The architecture, chemistry, and evolution of continental magmatic arcs, in Jeanloz, R., and Freeman, K. H., eds. *Annual Review of Earth and Planetary Sciences*, *43*, 299–331. https://doi.org/10.1146/annurev-earth-060614-105049

Gahalaut, V. K., Kundu, B., Laishram, S. S., Catherine, J., Kumar, A., Singh, M. D., et al. (2013). Aseismic plate boundary in the Indo-Burmese wedge, northwest Sunda Arc. *Geology*, *41*, 235–238. https://doi.org/10.1130/g33771.1

Garzanti, E., Radeff, G., & Malusà, M. G. (2018). Slab breakoff: A critical appraisal of a geological theory as applied in space and time. *Earth-Science Reviews*, *177*, 303–319. https://doi.org/10.1016/j.earscirev.2017.11.012

Guo, Z. F., Wilson, M., Liu, J., & Mao, Q. (2006). Post-collisional, potassic and ultrapotassic magmatism of the northern Tibetan Plateau: Constraints on characteristics of the mantle source, geodynamic setting and uplift mechanisms. *Journal of Petrology*, *47*, 1177–1220. https://doi.org/10.1093/petrology/egl007

Huang, X. X., Sun, Y., Yue, Y., Zhao, S., & Long, X. (2018). Determination of rhenium in geological samples by isotope dilution-multicollector-inductively coupled plasma-mass spectrometry with novel chromatographic separation. *Analytical Letters*, *51*, 1122–1146. https://doi.org/10.1080/00032719.2017.1371727

Ingle, S., Weis, D., Scoates, J. S., & Frey, F. A. (2002). Relationship between the early Kerguelen plume and continental flood basalts of the paleo-Eastern Gondwanan margins. *Earth and Planetary Science Letters*, *197*, 35–50. https://doi.org/10.1016/S0012-821x(02)00473-9

Ishikawa, A., Senda, R., Suzuki, K., Dale, C. W., & Meisel, T. (2014). Re-evaluating digestion methods for highly siderophile element and Os-187 isotope analysis: Evidence from geological reference materials. *Chemical Geology*, *384*, 27–46. https://doi.org/10.1016/j.chemgeo.2014.06.013

Ji, W.-Q., Wu, F.-Y., Chung, S.-L., Wang, X.-C., Liu, C.-Z., Li, Q.-L., et al. (2016). Eocene Neo-Tethyan slab breakoff constrained by 45 Ma oceanic island basalt-type magmatism in southern Tibet. *Geology*, *44*, 283–286. https://doi.org/10.1130/G37612.1

Jolivet, L., Faccenna, C., Becker, T., Tesauro, M., Sternai, P., & Bouilhol, P. (2018). Mantle flow and feforming continents: From India-Asia convergence to Pacific subduction. *Tectonics*, *37*, 2887–2914. https://doi.org/10.1029/2018TC005036

Katz, R. F., Spiegelman, M., & Langmuir, C. H. (2003). A new parameterization of hydrous mantle melting. *Geochemistry, Geophysics, Geosystems*, *4*(9), 1073. https://doi.org/10.1029/2002GC000433

Kelley, K. A., Plank, T., Newman, S., Stolper, E. M., Grove, T. L., Parman, S., & Hauri, E. H. (2010). Mantle melting as a function of water content beneath the Mariana arc. *Journal of Petrology*, *51*, 1711–1738. http://doi, https://doi.org/10.1093/petrology/egq036

Kind, R., & Yuan, X. (2010). Seismic images of the biggest crash on Earth. *Science*, *329*, 1479–1480. https://doi.org/10.1126/science.1191620

Kundu, B., & Gahalaut, V. K. (2012). Earthquake occurrence processes in the Indo-Burmese wedge and Sagaing fault region. *Tectonophysics*, *524-525*, 135–146. https://doi.org/10.1016/j.tecto.2011.12.031

Le Bas, M. J., Maitre, R. W. L., Streckeisen, A., & Zanettin, B. (1986). A chemical classification of volcanic rocks based on the total alkali-silica diagram. *Journal of Petrology*, *27*(3), 745–750. https://doi.org/10.1093/petrology/27.3.745

Lee, C.-T. A., Luffi, P., Plank, T., Dalton, H., & Leeman, W. P. (2009). Constraints on the depths and temperatures of basaltic magma generation on Earth and other terrestrial planets using new thermobarometers for mafic magmas. *Earth and Planetary Science Letters*, *279*, 20–33. https://doi.org/10.1016/j.epsl.2008.12.020

Lee, H.-Y., Chung, S.-L., Lo, C.-H., Ji, J., Lee, T.-Y., Qian, Q., & Zhang, Q. (2009). Eocene Neotethyan slab breakoff in southern Tibet inferred from the Linzizong volcanic record. *Tectonophysics*, *477*, 20–35. http://doi, https://doi.org/10.1016/j.tecto.2009.02.031

Lee, H.-Y., Chung, S.-L., & Yang, H.-M. (2016). Late Cenozoic volcanism in central Myanmar: Geochemical characteristics and geodynamic significance. *Lithos*, *245*, 174–190. https://doi.org/10.1016/j.lithos.2015.09.018

Lei, J., & Zhao, D. (2016). Teleseismic P-wave tomography and mantle dynamics beneath Eastern Tibet. *Geochemistry, Geophysics, Geosystems*, *17*, 1861–1884. https://doi.org/10.1002/2016GC006262

Li, C., van der Hilst, R. D., Meltzer, A. S., & Engdahl, E. R. (2008). Subduction of the Indian lithosphere beneath the Tibetan Plateau and Burma. *Earth and Planetary Science Letters*, *274*, 157–168. https://doi.org/10.1016/j.epsl.2008.07.016

Li, J.-X., Fan, W.-M., Zhang, L.-Y., Peng, T.-P., Sun, Y.-L., Ding, L., et al. (2020). Prolonged Neo-Tethyan magmatic arc in Myanmar: Evidence from geochemistry and Sr–Nd–Hf isotopes of Cretaceous mafic–felsic intrusions in the Banmauk–Kawlin area. *International Journal of Earth Sciences*, *109*, 649–668. https://doi.org/10.1007/s00531-020-01824-w

Licht, A., Dupont-Nivet, G., Win, Z., Swe, H. H., Kaythi, M., Roperch, P., et al. (2018). Paleogene evolution of the Burmese forearc basin and implications for the history of India-Asia convergence. *The Geological Society of America Bulletin*, *131*, 730–748. https://doi.org/10.1130/B35002.1

Lin, T.-H., Mitchell, A. H. G., Chung, S.-L., Tan, X.-B., Tang, J.-T., Oo, T., & Wu, F. Y. (2019). Two parallel magmatic belts with contrasting isotopic characteristics from southern Tibet to Myanmar: Zircon U-Pb and Hf isotopic constraints. *Journal of the Geological Society*, *176*, 574–587. https://doi.org/10.1144/jgs2018-072

Liu, C.-Z., Xu, Y., & Wu, F.-Y. (2018). Limited recycling of crustal osmium in forearc mantle during slab dehydration. *Geology*, *44*, 311–314. https://doi.org/10.1130/G37342.1

Liu, L., Gao, S., Liu, K. H., Li, S. Z., Tong, S. Y., & Kong, F. S. (2019). Toroidal mantle flow induced by slab subduction and rollback beneath the eastern Himalayan syntaxis and adjacent areas. *Geophysical Research Letters*, *46*, 11,080–11,090. https://doi.org/10.1029/2019GL084961

Luhr, J. F., & Haldar, D. (2006). Barren Island Volcano (NE Indian Ocean): Island-arc high-alumina basalts produced by troctolite contamination. *Journal of Volcanology and Geothermal Research*, *149*, 177–212. https://doi.org/10.1016/j.jvolgeores.2005.06.003

Mahéo, G., Guillot, S., Blichert-Toft, J., Rolland, Y., & Pêcher, A. (2002). A slab breakoff model for the Neogene thermal evolution of South Karakorum and South Tibet. *Earth and Planetary Science Letters*, *195*(1-2), 45–58. https://doi.org/10.1016/s0012-821x(01)00578-7

Mahoney, J. J., Natland, J. H., White, W. M., Poreda, R., Bloomer, S. H., Fisher, R. L., & Baxter, A. N. (1989). Isotopic and geochemical provinces of the western Indian Ocean spreading centers. *Journal of Geophysical Research*, *94*(B4), 4033–4052. https://doi.org/10.1029/JB094iB04p04033

Maurin, T., Masson, F., Rangin, C., Min, U. T., & Collard, P. (2010). First global positioning system results in northern Myanmar: Constant and localized slip rate along the Sagaing fault. *Geology*, *38*, 591–594. https://doi.org/10.1130/G30872.1

Maurin, T., & Rangin, C. (2009). Structure and kinematics of the Indo-Burmese Wedge: Recent and fast growth of the outer wedge. *Tectonics*, *28*, TC2010. https://doi.org/10.1029/2008tc002276

Maury, R. C., Pubellier, M., Rangin, C., Wulput, L., Cotten, J., Socquet, A., et al. (2004). Quaternary calc-alkaline and alkaline volcanism in an hyper-oblique convergence setting, central Myanmar and western Yunnan. *Bulletin de la Societe Geologique de France*, *175*, 461–472. https://doi.org/10.2113/175.5.461

McBride, J. S., Lambert, D. D., Nicholls, I. A., & Price, R. C. (2001). Osmium isotopic evidence for crust–mantle interaction in the genesis of continental intraplate basalts from the Newer Volcanics Province, southeastern Australia. *Journal of Petrology*, *42*(6), 1197–1218. https://doi.org/10.1093/petrology/42.6.1197

McCaffrey, R. (1992). Oblique plate convergence, slip vectors, and forearc deformation. *Journal of Geological Research*, *97*(B6), 8905–8915. https://doi.org/10.1029/92JB00483

Meschede, M. (1986). A method of discriminating between different types of mid-ocean ridge basalts and continental tholeiites with the Nb-Zr-Y diagram. *Chemical Geology*, *56*(3-4), 207–218. https://doi.org/10.1016/0009-2541(86)90004-5

Mitchell, A. H. G. (1993). Cretaceous–Cenozoic tectonic events in the western Myanmar (Burma)-Assam region. *Journal of the Geological Society*, *150*(6), 1089–1102. https://doi.org/10.1144/gsjgs.150.6.1089

Mitchell, A. H. G., Chung, S.-L., Oo, T., Lin, T.-H., & Hung, C.-H. (2012). Zircon U-Pb ages in Myanmar: Magmatic-metamorphic events and the closure of a neo-Tethys ocean? *Journal of Asian Earth Sciences*, *56*, 1–23. https://doi.org/10.1016/j.jseaes.2012.04.019

Morley, C. K., & Arboit, F. (2019). Dating the onset of motion on the Sagaing fault: Evidence from detrital zircon and titanite U-Pb geochronology from the North Minwun Basin, Myanmar. *Geology*, *47*, 581–585. https://doi.org/10.1130/G46321.1

Ni, J. F., Guzman-Speziale, M., Bevis, M., Holt, W. E., Wallace, T. C., & Seager, W. R. (1989). Accretionary tectonics of Burma and the three-dimensional geometry of the Burma subduction zone. *Geology*, *17*(1), 68–71. https://doi.org/10.1130/0091-7613(1989)0172.3.CO;2

Niu, Y. (2017). Slab breakoff: A causal mechanism or pure convenience? *Science Bulletin*, *62*, 456–461. https://doi.org/10.1016/j.scib.2017.03.015

Pearce, J. A. (2008). Geochemical fingerprinting of oceanic basalts with applications to ophiolite classification and the search for Archean oceanic crust. *Lithos*, *100*, 14–48. https://doi.org/10.1016/j.lithos.2007.06.016

Peccerillo, A., & Taylor, S. R. (1976). Geochemistry of Eocene calc-alkaline volcanic rocks from the Kastamonu area, northern Turkey. *Contributions to Mineralogy and Petrology*, *58*(1), 63–81. https://doi.org/10.1007/bf00384745

Pesicek, J. D., Thurber, C. H., Zhang, H., DeShon, H. R., Engdahl, E. R., & Widiyantoro, S. (2010). Teleseismic double-difference relocation of earthquakes along the Sumatra-Andaman subduction zone using a 3-D model. *Journal of Geophysical Research*, *115*, B10303. https://doi.org/10.1029/2010JB007443

Plank, T., & Langmuir, C. H. (1998). The chemical composition of subducting sediment and its consequences for the crust and mantle. *Chemical Geology*, *145*(3–4), 325–394. https://doi.org/10.1016/S0009-2541(97)00150-2

Prelević, D., Akal, C., Romer, R. L., Mertz-Kraus, R., & Helvac, C. (2015). Magmatic response to slab tearing: Constraints from the Afyon alkaline volcanic complex, western Turkey. *Journal of Petrology*, *56*, 527–562. http://doi.10.1093/petrology/egv008

Rabbel, W., Koulakov, I., Dinc, A. N., & Jakovlev, A. (2011). Arc-parallel shear deformation and escape flow in the mantle wedge of the Central America subduction zone: Evidence from P wave anisotropy. *Geochemistry, Geophysics, Geosystems*, *12*, Q05S31. https://doi.org/10.1029/2010GC003325

Raju, K. A., Ramprasad, T., Rao, P. S., Ramalingeswara Rao, B., & Varghese, J. (2004). New insights into the tectonic evolution of the Andaman basin, northeast Indian Ocean. *Earth and Planetary Science Letters*, *221*, 145–162. https://doi.org/10.1016/S0012-821x(04)00075-5

Rangin, C., Maurin, T., & Masson, F. (2013). Combined effects of Eurasia/Sunda oblique convergence and East-Tibetan crustal flow on the active tectonics of Burma. *Journal of Asian Earth Sciences*, *76*, 185–194. https://doi.org/10.1016/j.jseaes.2013.05.018

Rao, N. P., & Kumar, M. R. (1999). Evidences for cessation of Indian plate subduction in the Burmese arc region. *Geophysical Research Letters*, *26*(20), 3149–3152. https://doi.org/10.1029/1999GL005396

Reisberg, L., Zindler, A., Marcantonio, F., White, W., Wyman, D., & Weaver, B. (1993). Os isotope systematics in ocean island basalts. *Earth and Planetary Science Letters*, *120*(3-4), 149–167. http://10.1016/0012-821x(93)90236-3, https://doi.org/10.1016/0012-821X(93)90236-3

Replumaz, A., Negredo, A. M., Guillot, S., & Villasenor, A. (2010). Multiple episodes of continental subduction during India/Asia convergence: Insight from seismic tomography and tectonic reconstruction. *Tectonophysics*, *483*, 125–134. https://doi.org/10.1016/j.tecto.2009.10.007

Rudnick, R. L., & Gao, S. (2003). Composition of the continental crust. In H. D. Holland, & K. K. Turekian (Eds.), Treatise on geochemistry (pp. 1–64). Amsterdam: Elsevier.

Saal, A. E., Rudnick, R. L., Ravizza, G. E., & Hart, S. R. (1998). Re-Os isotope evidence for the composition, formation and age of the lower continental crust. *Nature*, *393*(6680), 58–61. https://doi.org/10.1038/29966

Searle, M. P., Noble, S. R., Cottle, J. M., Waters, D. J., Mitchell, A. H. G., Hlaing, T., & Horstwood, M. S. A. (2007). Tectonic evolution of the Mogok metamorphic belt, Burma (Myanmar) constrained by U-Th-Pb dating of metamorphic and magmatic rocks. *Tectonics*, *26*, TC3014. https://doi.org/10.1029/2006TC002083

Shi, D. N., Wu, Z. H., Klemperer, S. L., Zhao, W. J., Xue, G. Q., & Su, H. (2015). Receiver function imaging of crustal suture, steep subduction, and mantle wedge in the eastern India-Tibet continental collision zone. *Earth and Planetary Science Letters*, *414*, 6–15. https://doi.org/10.1016/j.epsl.2014.12.055

Shirey, S. B., & Walker, R. J. (1998). The Re-Os isotope system in cosmochemistry and high-temperature geochemistry. *Annual Review of Earth and Planetary Sciences*, *26*(1), 423–500. https://doi.org/10.1146/annurev.earth.26.1.423

Sibuet, J.-C., Klingelhoefer, F., Huang, Y.-P., Yeh, Y.-C., Rangin, C., Lee, C.-S., & Hsu, S. K. (2016). Thinned continental crust intruded by volcanics beneath the northern Bay of Bengal. *Marine and Petroleum Geology*, *77*, 471–486. https://doi.org/10.1016/j.marpetgeo.2016.07.006

Sippl, C., Schurr, B., Yuan, X., Mechie, J., Schneider, F. M., Gadoev, M., et al. (2013). Geometry of the Pamir-Hindu Kush intermediate-depth earthquake zone from local seismic data. *Journal of Geophysical Research: Solid Earth*, *118*, 1438–1457. https://doi.org/10.1002/jgrb.50128

Stephenson, D., & Marshall, T. R. (1984). The petrology and mineralogy of Mt. Popa volcano and the nature of the late-Cenozoic Burma volcanic arc. *Journal of the Geological Society*, *141*(4), 747–762. https://doi.org/10.1144/gsjgs.141.4.0747

Sun, S.-S., & McDonough, W. F. (1989). Chemical and isotopic systematics of oceanic basalts: Implications for mantle composition and processes. *Geological Society, London, Special Publications*, *42*(1), 313–345. https://doi.org/10.1144/GSL.SP.1989.042.01.19

Syacuse, E. M., & Abers, G. A. (2007). Global compilation of variations in slab depth beneath arc volcanoes and implications. *Geochemistry, Geophysics, Geosystems*, *7*, Q05017. https://doi.org/10.1029/2005GC001045

Tian, H.-C., Yang, W., Li, S.-G., Ke, S., & Duan, X.-Z. (2018). Low δ^{26}Mg volcanic rocks of Tengchong in southwestern China: A deep carbon cycle induced by supercritical liquids. *Geochimica et Cosmochimica Acta*, *240*, 191–219. https://doi.org/10.1016/j.gca.2018.08.032

Völkening, J., Köppe, M., & Heumann, K. G. (1991). Tungsten isotope ratio determinations by negative thermal ionization mass spectrometry. *International Journal of Mass Spectrometry and Ion Processes*, *107*, 361–368. https://doi.org/10.1016/0168-1176(91)80070-4

von Blanckenburg, F., & Davies, J. H. (1995). Slab breakoff: A model for syncollisional magmatism and tectonics in the Alps. *Tectonics*, *14*, 120–131. https://doi.org/10.1029/94tc02051

Wang, C. Y., Flesch, L. M., Silver, P. G., Chang, L. J., & Chan, W. W. (2008). Evidence for mechanically coupled lithosphere in central Asia and resulting implications. *Geology*, *36*, 363–366. https://doi.org/10.1130/G24450a.1

Wang, J.-G., Wu, F.-Y., Tan, X.-C., & Liu, C.-Z. (2014). Magmatic evolution of the Western Myanmar Arc documented by U–Pb and Hf isotopes in detrital zircon. *Tectonophysics*, *612-613*, 97–105. https://doi.org/10.1016/j.tecto.2013.11.039

Wang, Q., Hawkesworth, C. J., Wyman, D., Chung, S. L., Wu, F. Y., Li, X. H., et al. (2016). Pliocene–Quaternary crustal melting in central and northern Tibet and insights into crustal flow. *Nature Communications*, *7*, 11888. https://doi.org/10.1038/ncomms11888

Wang, Y. Q., Huang, X. X., Sun, Y. L., Zhao, S., & Yue, Y. H. (2017). A new method for the separation of light rare earth elements in geological materials using a single column containing TODGA resin and its application to the determination of Nd isotope compositions by multicollector inductively coupled plasma-mass spectrometry. *Analytical Methods*, *9*, 3531–3540. https://doi.org/10.1039/C7AY00966

Wilson, M. (1989). *Igneous Petrogenesis* (pp. 1–466). London: Unwin Hyman. https://doi.org/10.1007/978-1-4020-6788-4

Wood, D. A. (1980). The application of a Th-Hf-Ta diagram to problems of tectonomagmatic classification and to establishing the nature of crustal contamination of basaltic lavas of the British Tertiary Volcanic Province. *Earth and Planetary Science Letters*, *50*(1), 11–30. https://doi.org/10.1016/0012-821x(80)90116-8

Wortel, M., & Spakman, W. (2000). Subduction and slab detachment in the Mediterranean-Carpathian region. *Science*, *290*(5498), 1910–1917. https://doi.org/10.1126/science.290.5498.1910

Xu, Q., Zhao, J. M., Yuan, X. H., Liu, H. B., & Pei, S. P. (2017). Detailed configuration of the underthrusting Indian lithosphere beneath western Tibet revealed by receiver function images. *Journal of Geophysical Research: Solid Earth*, *122*, 8257–8269. https://doi.org/10.1002/2017jb014490

Yang, D. (2011). *The $^{40}Ar/^{39}$ Ar geochronology and geochemistry research on Cenozoic volcanic rocks of Hoh Xil and Kunlun in the northern Tibetan Plateau*. (PhD thesis, pp. 1–141) (In Chinese with English abstract). Beijing: Graduate University of Chinese Academy Sciences.

Yin, A., & Harrison, T. M. (2000). Geologic evolution of the Himalayan-Tibetan orogen. *Annu. Rev. Annual Review of Earth and Planetary Sciences*, *28*(1), 211–280. https://doi.org/10.1146/annurev.earth.28.1.211

Yoshioka, S., & Wortel, M. J. R. (1995). Three-dimensional numerical modeling of detachment of subducted lithosphere. *Journal of Geophysical Research*, *100*(B10), 20,223–20,244. https://doi.org/10.1029/94jb01258

Zhang, J. E., Xiao, W., Windley, B. F., Wakabayashi, J., Cai, F., Sein, K., et al. (2018). Multiple alternating forearc- and backarc-ward migration of magmatism in the Indo-Myanmar Orogenic Belt since the Jurassic: Documentation of the orogenic architecture of eastern Neotethys in SE Asia. *Earth-Science Reviews*, *185*, 704–731. https://doi.org/10.1016/j.earscirev.2018.07.009

Zhang, P.-Z., Shen, Z., Wang, M., Gan, W., Bürgmann, R., Molnar, P., et al. (2004). Continuous deformation of the Tibetan Plateau from global positioning system data. *Geology*, *32*, 809–812. https://doi.org/10.1130/G20554.1

Zhao, J., Yuan, X., Liu, H., Kumar, P., Pei, S., Kind, R., et al. (2010). The boundary between the Indian and Asian tectonic plates below Tibet. *Proceedings of the National Academy of Sciences of the United States of America*, *107*, 11,229–11,233. https://doi.org/10.1073/pnas.1001921107

Zhao, W. J., Kumar, P., Mechie, J., Kind, R., Meissner, R., Wu, Z. H., et al. (2011). Tibetan plate overriding the Asian plate in central and northern Tibet. *Nature Geoscience*, *4*, 870–873. https://doi.org/10.1038/Ngeo1309

Zhou, M.-F., Robinson, P. T., Wang, C. Y., Zhao, J.-H., Yan, D.-P., Gao, J.-F., & Malpas, J. (2011). Heterogeneous mantle source and magma differentiation of Quaternary arc-like volcanic rocks from Tengchong, SE margin of the Tibetan Plateau. *Contributions to Mineralogy and Petrology*, *163*, 841–860. https://doi.org/10.1007/s00410-011-0702-8

Zhu, D. C., Chung, S. L., Mo, X. X., Zhao, Z. D., Niu, Y., Song, B., & Yang, Y. H. (2009). The 132 Ma Comei-Bunbury large igneous province: Remnants identified in present-day southeastern Tibet and southwestern Australia. *Geology*, *37*, 583–586. https://doi.org/10.1130/G30001a.1

Zhu, D. C., Wang, Q., Zhao, Z. D., Chung, S. L., Cawood, P. A., Niu, Y., et al. (2015). Magmatic record of India-Asia collision. *Scientific Reports*, *5*, 14289. https://doi.org/10.1038/srep14289